3 Theoretical and Experimental Principles

In the following Chapter some of the basic knowledge and conditions will be presented that are not necessarily present in chemical or mechanical engineering and not even in textile machinery construction. These are also difficult to find in the literature. An example for this is the unit 1 tex = 1 g/1000 m yarn that is a weight unit but at the same time (because the specific weight of the yarn material is constant) is also often used as a unit for the cross-section (see Chapter 10).

3.1 Reactors for Production and/or Dissolving

3.1.1 Selection Criteria

The diversity of machine design according to Chapter 2 can be simplified by combining similar groups that allow optimization within each group [1]. The processes usually involve a significant increase in viscosity (from < 1 P to several $10^3 \ldots 10^5$ P). Other materials that cannot be dissolved in each other (e.g., TPA in ethylene glycol) require specific preparation for intimate mixtures. Also for the equipment dimensions there is an analogy rule that is defined by the non-dimensional Damköhler number [2]:

$$Dz = C_{A0} \cdot k_A \cdot \exp(-E_A/RT) \cdot z_m \tag{3.1}$$

with

C_{AO} = Starting concentration of the final component A
k_A = Factor for the reaction speed
E_A = Energy for activation
R = Gas constant
T = Temperature [K]
z_m = Average duration = Volume/throughput

With continuously running sequential reactors of same vessel diameter the throughput is the lowest in the ideally mixed single stirring vessel. It increases with more vessels to reach the ideal flow tube in the case of an infinite number in the stirring vessel cascade. This again is equal to the ideally mixed discontinuous single stirring vessel. This also is equal to the maximum throughput in a reactor [2]. Thus the average duration z_m also increases for a larger reactor. Table 3.1 shows that near 100% throughput the duration in the vessel closely approximates to the duration in the ideally mixed single stirrer vessel. In the case of a vessel cascade it should be considered if with the desired throughput per vessel the overall duration is not unnecessarily extended. Many technical processes are therefore stopped at 60 ... 65% of the throughput, and the unchanged raw material is e.g., evaporated, recycled and reused in the initial step.

The reactor type according to Fig. 3.1, left, has significant influence on the histogram of the concentration (=answer at the reactor exit to an impact marking) and the sum diagram (=answer to a crack marking). Additionally the approximate duration distribution for a reactor screw is mentioned.

For many polymer formation reactions in addition to the main reaction there are parallel or subsequent reactions that influence the molecular weight distribution and the like. Even concentration distribution and a narrow temperature and time range result in the best conditions. The ideal flow tube

Table 3.1 Necessary Residence Time in Relation to the Vessel Optimized for Mixing Efficiency (= 1)

Throughput in %	Dwell time factor
80	5
90	10
99.5	200
99.9	1000

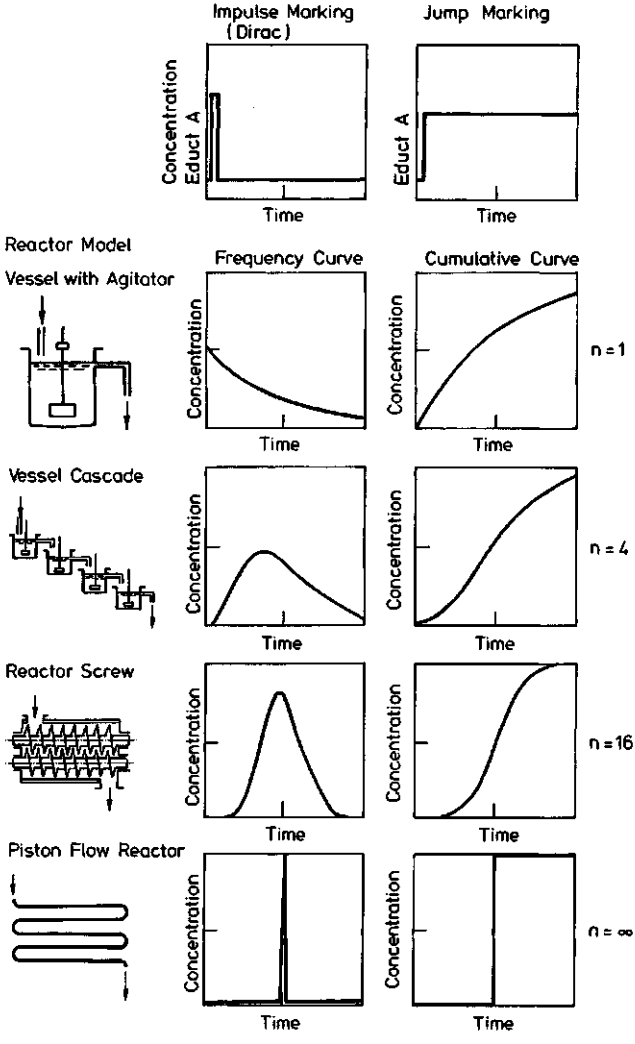

Figure 3.1
Dwell time distribution for different reactor models and comparison with a reactor screw [2] (frequency curve in response to an impact marking [2, 3]

comes closest to this, followed by the double screw reactor with circumference tubes that are as close as possible to each other.

A comparison of different reactors and/or process conditions permit the following numbers that need to be calculated and compared to each other or a benchmark:

- the average duration or the throughput
- the distribution of the duration or the reverse mixing
- the distribution intensity, radial and as a function of time
- the temperature arrangement and distribution
- the specific heat transfer surface (e.g., m^2/dm^3 volume)
- the pressure area and the pressure arrangement (including a possible vacuum)
- the degassing efficiency
- the power of the stirrer/agitator drive
- self-cleaning and disturbing coats
- the discharge

Good distribution and dispersing intensities require specific mixing and shearing elements. For example for high viscose products these should maximize the product of shearing speed × duration; this can be measured over the stirrer drive torque or by the stirrer power/filling volume [kW/m^3]. Low viscose products require high turbulence.

The average duration of continuous reactors depends on

- the rpm of the screw
- the empty volume respectively the geometry and the filling percentage.

Table 3.2 recommends some dimensions (also see Chapter 4.1 and 4.2).

Table 3.2 Dimensions for Reactors

	Specific power or data
Difficult disintegration for	
continuous processes	0.1 . . . 0.5 kWh/kg throughput
discontinuous processes	≈0.3 kWh/kg content
Simple disintegration in high viscous phase	
continuous	0.02 . . . 0.15 kWh/kg throughput
discontinuous	≈0.3 kWh/kg content
Heat dissipation at 1.5 kJ/kg K	≤≈0.2 K/s (adiabatic)
Heat transfer area	> 0.1 m^2/dm^3, isothermic temperature guidance
	< 0.01 m^2/dm^3, only approximate adiabatic temperature guidance
Heat transfer coefficients	50 . . . 500 W/m^2 K
Pressure (usual limits)	0.05 mbar to 35 bar
Stirrer drives for < 1000 P	
discontinuous	≤ 0.005 kWh/kg
continuous	≤ 0.02 kWh/kg
1000 . . . 10,000 P	≈0.5 kWh/kg
Clearance between stirrer and inside wall	
for self cleaning	0.001 × D [mm] ≥ 1 mm
for one shaft reactors	0.0005 × D [mm] < 0.2 mm

For continuous reactors the usual duration is between a few and 240 min; it may be as high as 20 h. For discontinuous processes the duration is usually between 5 min and 20 h, but can be set as needed. In addition to this there are the times for filling and emptying that can take 1 . . . 30 min each for the bigger autoclaves, while their content participates in the reaction, thus increasing the dispersing and/or causing a certain degradation of the finished product, for example when discharging PA 66.

3.1.2 Preferred Reactor Cascades

For major viscosity changes or after vacuum and pressure areas it is recommended to separate the several sequential autoclaves. Examples for this are:

- PAN solution polymerization: In the first autoclave the salts are dissolved in water or solvent and the monomers are mixed in, in the second autoclave polymerization occurs, in the third autoclave the not transformed monomers (about 30...40%) are evaporated to recycling before the product discharge (Fig. 2.96).
- Autoclave polycondensation of PA 66 (Fig. 2.29): In the first vessel the solution is prepared and in the second it is prepolycondensated, starting with about 20 bar and decreasing pressure to about 2 bar; the third autoclave serves for finish-polycondensation with a pressure decrease from about 2 bar to normal pressure and extrusion.
- Autoclave polycondensation to PET (Fig. 2.44): Two parallel entry autoclaves serve to prepare DMT and ethylene glycol, a second for transesterification at 1 (possibly up to 6) bar; in the third autoclave polycondensation occurs at up to 0.1 mbar and about 3000 P with subsequent melt extrusion at up to 10 bar in 30 min maximum.
- Continuous polycondensation of DEG to PET (Fig. 2.50b): First autoclave at 80...100 mbar, second autoclave at 50...20 mbar, third reactor as finisher at about 0.5 mbar with the transports between these by the vacuum difference.
- Continuous polycondensation of TPA and EG to PET (Fig. 2.3): The first and possibly the second autoclave serve to mix and ester to DEG at up to 10 bar; the second, third and fourth autoclave with 80 respectively 8 respectively 2 mbar are for the pre-polymerization, and in the fifth reactor (=finisher) the product is finished at about 0.5 mbar and then extruded by means of a pump.
- PAN solution preparation (Fig. 2.49): Two high shear mixers that work alternating allow the preparation of the emulsion from powder and solvent; the second autoclave is used for dissolving, the third for degassing, and the fourth for homogenization before passing ahead.

Preferred are also vessel cascades with 2 to 4 autoclaves in a row, for low viscous liquids with dished bottom, high speed mixer, for liquids that do not require intensive mixing and for those above 400 P with a conical bottom and anchor agitator. At 2500...5000 P the spiral anchor agitators with an incline of about $1\,D$ and at 10,000...15,000 P with an incline of about $1/3\,D$ are preferred. For >30,000...50,000 P double cone mixers (Fig. 2.119) or Z-kneaders are preferable. For even higher viscosities double screw mixers are suited.

3.1.3 Reactor Design [3]

With an increase in size of the reactor autoclaves the ratio of heat exchange vessel surface to filling volume becomes smaller. For the usual autoclave depth of $(1...1.5)\,D$ for example the ratio of contact surface to volume changes as $O_K/V = (1/H) + (4/D)$; it is for 25 l about 16, for 1 m^3 about 4, at 2 m^3 about 2 and for 6 m^3 about 0.8; this requires special measures for the heat induction and cooling. This is done by inner heating and cooling coils (Fig. 4.106) or heating and cooling cylinders (Fig. 2.45) or built-in heat exchange surfaces (Fig. 4.10b and 2.45) or higher Reynolds numbers. The latter can only be obtained through a higher torque moment.

The necessary vessel size results from:

$$V_K \approx 1.05 \cdot (1 + k) \cdot V_P/f \tag{3.2}$$

with V_P = production volume, e.g., for 2 t PET/lot with 1.2 kg/dm^3 about 4.1 m^3 vessel volume, $k = 0.72$ kg EG/kg PET and f initial filling degree ≈ 0.7). If foaming is feared, $f \approx 0.5...0.6$ or for pure monomers (e.g., caprolactam) $f < \approx 0.8$. Since in the subsequent polycondensation autoclave already 0.31 kg less methanol/kg PET enter, the volume can be smaller accordingly: about 3.7 m^3.

For the continuous process the polymer fiber industry primarily uses:

- the VK tube (simplified continuous polymerization, Fig. 2.18 to 2.20) [4] for the production of PA 6. This is a piston flow reactor because the horizontal speed and temperature distribution are kept quite

constant through installations. The sizes are between 200 l (=200 mm diameter × 6500 mm length) and about 20 m^3 (=about 1600 mm diameter × 10,000 mm length). Due to the low heat conductivity of the melt, diameters of over 300 mm require inside heat exchangers (Fig. 2.20).

- the single shaft vertical paddle reactor where the solution or melt flows down the inside wall of a heated tube and is continuously turned and moved out by a paddle rotor [5]. It is mostly used for the evaporation of solvents, but also for the evaporation of monomers from PA 6 or the evaporation of glycol from PET from a too small reaction surface.
- the horizontal single shaft screw reactor (Fig. 2.21) or the horizontal rotating reactor (position 11 in Fig. 2.49 respectively Fig. 2.52 and 2.53): The rotor continuously moves melt from the sump upwards and it then flows freely back down and evaporates from the surface. Thus you easily obtain 40 m^2 film surface with 1 m diameter and 4.5 m length that works on both sides and results in high evaporation rates. For viscosities above about 3000 P these must be built very sturdy as they turn the melt more and cause less film formation the higher the viscosity (Fig. 2.52).
- the two shaft paddle reactor (Fig. 2.47, 2.51): It corresponds very much to the double screw extruder, but has much more clearance between the screws and generally a larger volume. They are built with screw diameters of up to 800 mm × 30 D length. Even tempering is common, sometimes also for the screw shaft and the rotors. With short ram zones they can be separated into different pressure zones, especially for high viscous materials.

The variety of the described reactors requires careful selection unless it is possible to use known reactor types for specific processes. Because of the high cost it is recommended to run pilot plant trials first.

3.2 The Spinning Mechanism

3.2.1 General View over Melt Spinning

A very detailed description by *Ziabicki* [8] exists as well as two brief summaries [9, 10], so that it is quite sufficient to briefly show the physical process from the spinneret to the first take-up point. The fluid mechanical processes of the high viscous fluids and their change to the solid state as well as the changing rheological properties of the non-Newtonian liquids that are structurally viscous and visco-elastic, make the mathematical treatment more difficult.

Important spinning conditions are:

- macromolecular chains with a minimum of branches and networks with more than a minimum degree of polymerization
- sufficient ability of the melted mass to be drawn into filaments, as for example defined by the filament breaking length. The latter depends on the viscosity η and the draft velocity v (see Fig. 3.2a) [11]. The maximum indicates the optimum spinnability of the material [12]. The breaking length $L = f(v \cdot \eta)$ is limited by the melt fracture and the breaking of the filaments (see Fig. 3.3b). Too high a take-up speed and/or too low a viscosity leads to breaking filaments (e.g. due to too thin melt or too high spinning temperatures). Too high molecular weights or viscosity or too fast hardening or coagulation of the outer layer lead to a melt fracture, e.g. melting rupture (=saw toothed appearance).

When the melt enters the spinneret openings we are dealing with creeping flow with Reynolds numbers in the range of 10^{-7}. Inside the spinneret's capillaries 0.2 ... 1 m/s are achieved, respectively Re = 0.01 ... 0.2. After exiting the capillary the average speed is reduced due to the spinneret swell by 1.1 to 2 times, and then increases with the cooling and solidification of the filament to the take-up speed. The uneven velocity distribution inside the spinneret bore (see Fig. 4.87) is due to the sticking of the solution in a thin area near the wall (range of 0.01 ... 0.02 mm), and directly upon exiting it changes to a constant speed over the cross-section, and then increases upon cooling from the outside to the inside up to the take-up speed (see Fig. 3.3b). The flow in the liquid state is described by the elongation viscosity; this is certainly not correct for non-Newtonian liquids, but to date has not been completely investigated.

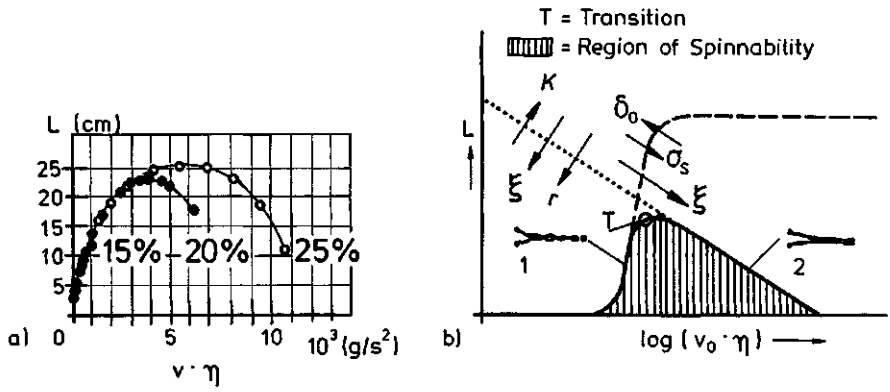

Figure 3.2 *a*) Maximum length L [cm] of the fluid thread as a function of the extrusion velocity v and the shear viscosity η; The extrudates are differently concentrated solutions of cellulose acetate $[n] = 1.92\,\mathrm{dl\,g^{-1}}$ in an acetone water mixture of 85 : 15 volume-%: L_{max} results in good spinnability
b) Superposition of theoretical curves of capillary wave failure. (- - - -) and cohesion failure (· · · ·). Maximum length of the fluid filament is plotted as a function of the product of extrusion velocity v_0 and shear viscosity η; d_0 = initial diameter; $\xi = d\ln(v/v_0)/dx$ = axial deformation gradient; σ_S = surface tension; K = energy of cohesion; τ = relaxation time = time for the stress (stored energy) created by a sudden deformation to decay to the (1/e)-part [10]; the arrow shows the direction in which the theoretical curves shift when the indicated parameter increases

For the common spinning of filaments in the finished range of about 1 . . . 20 dtex (≈0.01 . . . 0.05 mm diameter) spinnerets of a diameter of 0.05 . . . 0.25 mm are used for solution spinning, and 0.1 . . . 0.7 mm for melt spinning. The capillary length is $L = (1 \ldots 4)D$, in some cases up to about $10D$. The question concerning the optimum prebore—cylindrical, conical, double conical, hyperbolical [14]—has not yet been determined.

Figure 3.3a shows what happens inside the filament after exiting the spinneret, and Fig. 3.3b shows the schematic changes in the filament properties until the material has solidified.

Melt spinning is done for most polymers (PA, PET, PP et similes) between 240 and 320 °C, for some special polymers under 200 °C or between 350 and 450 °C, usually under high pressure (100 . . . 200 bar) through very thick spinneret plates (= 10 mm, see chapter 4 and the accompanying figures). In each position x of the thread way the following is valid:

$$\gamma \times F(x) \times v(x) = G = \text{constant} \tag{3.2}$$

with γ = density of the polymer (melt or solid), F = filament cross-section, v = filament speed, and G = throughput/bore. For a round filament cross-section $F = d^2\pi/4$ (d = filament diameter) and

$$d(x) = 2\sqrt{G/\pi \cdot \gamma \cdot v(x)} \tag{3.3}$$

Table 3.3 shows some general values from operation.

The extrusion velocity = exit velocity from the spinneret v_B[m/min] follows of

$$v_B = 4 \times G_B/\pi \times D^2 \times \gamma_{melt} \tag{3.4}$$

with G_B[g/min] filament mass per hole, D [mm] capillary diameter, γ = density of the melt [g/cm³]; for spinning 167 dtex f 36 PET-POY this will result with $D = 0.3$ mm, $v_{sp} = 3600$ m/min, $i = 1.44$: $v_B = 28.4$ m/min.

This will result in the

$$\text{Spin draft} = \text{take-up speed/extrusion speed} = v_{sp}/v_B \tag{3.5}$$

In this example this would be 126.76 (see Fig. 2.58).

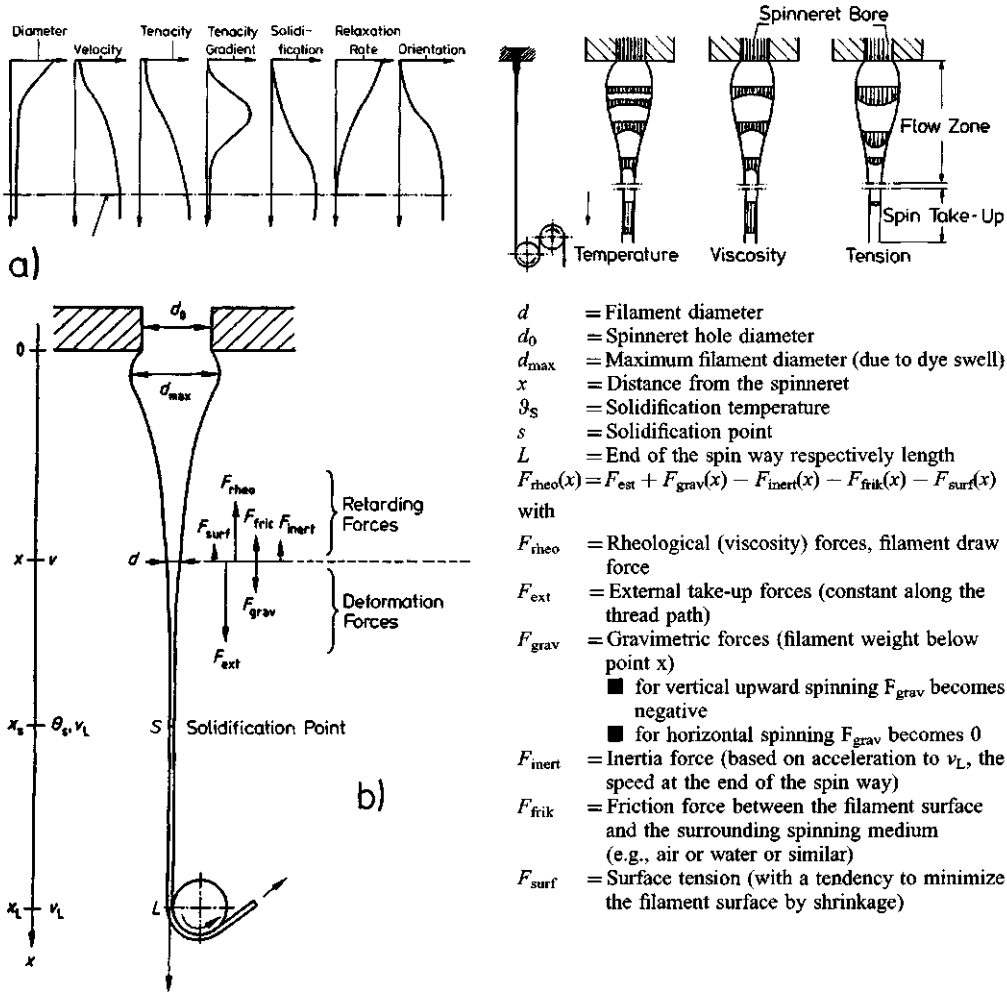

d = Filament diameter
d_0 = Spinneret hole diameter
d_{max} = Maximum filament diameter (due to dye swell)
x = Distance from the spinneret
ϑ_S = Solidification temperature
s = Solidification point
L = End of the spin way respectively length
$F_{rheo}(x) = F_{ext} + F_{grav}(x) - F_{inert}(x) - F_{frik}(x) - F_{surf}(x)$
with
F_{rheo} = Rheological (viscosity) forces, filament draw force
F_{ext} = External take-up forces (constant along the thread path)
F_{grav} = Gravimetric forces (filament weight below point x)
- for vertical upward spinning F_{grav} becomes negative
- for horizontal spinning F_{grav} becomes 0

F_{inert} = Inertia force (based on acceleration to v_L, the speed at the end of the spin way)
F_{frik} = Friction force between the filament surface and the surrounding spinning medium (e.g., air or water or similar)
F_{surf} = Surface tension (with a tendency to minimize the filament surface by shrinkage)

Figure 3.3 *a*) Temperature, viscosity and tension distribution in the polymer stream and schematic curves of different filament situations and properties during the melt spinning process
b) Force equilibrium of the spinning filament (yarn direction downwards)

During melt spinning the following phenomena need to be observed:

- In high pressure extrusion the melt pressure of usually more than 400 bar between the extruder screw tip, extrusion pump and extrusion pack is reduced by friction in the extrusion pack to the necessary entrance pressure at the spinneret filter of usually 20 to 60 bar. Specific slots or filters in the extrusion pack are suitable for this. Filters, however, will change the pressure with running time and clogging. Due to the sheering force, frictional heat is developed, increasing the melt temperature of PET or PA by 4 . . . 4.2 K per 100 bar pressure drop (see Fig. 3.4). Because there are only a few seconds between this increase in temperature to the cooling of the filament, the temperature increase is usually without risk for the polymer. With proper control of the melt flow one can achieve a uniform heating over the cross-section of the melt and thus an increase of the exit temperature, a decrease of the melt viscosity

Table 3.3 Examples for the Yarn Take-Up from the Spinneret, etc.

Yarn	Material	Take-up	$i_{(residual\ shrinkage)}$	ς_{melt}	ς_{solid}	Spinneret hole diameter	Individual spinning titer	$v_{spinneret\ hole}$	G	Draw ratio	Individual filament diameter	
											finished	undrawn
dtex		m/min		g/cm³	g/cm³	mm	dtex	m/min	g/min		µm	µm
Staple fiber/1.75	PET	1500	3.4	1.25	1.34	0.3	5.95	10.103	0.8925	148.5	12.85	23.69
167/f52		3500	1.4				4.496	17.81	1.5736	196.5	17.4	
50/f100		3200	1.4			0.2	0.7	5.704	0.224	561.0	6.87	8.13
1380/f230		620	5.4			0.45	32.4	10.10	2.009	61.4	25.8	
1380/f230	PA 6	620	4.0	1.00	1.14	0.4	24	11.84	1.488	52.4	25.89	
1380/f82	PP	600	3.4	0.7	0.91	0.8	57.22	9.76	3.433	61.5	200.1	369
70/f27	PA 6	1200	3.4	1.0	1.14	0.25	8.815	21.55	1.058	55.7	17.0	
	PA66					0.20		33.68	1.058	35.6	17.0	
30/f11		5600	1.2	1.0	1.14	0.20	3.273	58.35	1.833	95.98	17.46	
167/f52	PP	3400	1.7	0.75	0.91	0.3	5.46	35.01	1.856	97.1	21.31	
Staple fiber/1.75		40	4	0.7	0.91	0.3	7.0	0.566	0.028	70.6	15.73	31.46
/15		30	4	0.7	0.91	0.7	60.0	0.668	0.18	44.9	46.0	92.1
3.0 (dry)	PAN	400	4	$\varsigma_{solution}$ 1.1	1.27	0.3	12(48)	(24.69)	0.48	(64.8)		
3.0 (wet)		12				0.08	12(48)	(10.42)	0.0144	(1.12)		

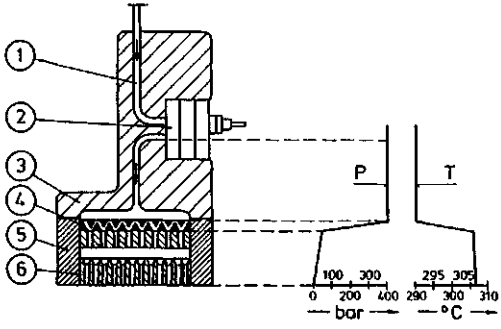

Figure 3.4
Principle of the high pressure spinning process
1 Melt supply
2 High pressure spinning pump
3 Zone of lower melt temperature
4 Filter and/or decompression mechanism
5 Zone of higher temperature
6 Spinneret
p Pressure course of the polymer
T Temperature course of the polymer
} both caused by energy transformation of the friction loss into melt heating

and an improvement of the spinning conditions, especially for high viscous materials. The spinneret temperature, e.g. of the Dow vapor, stays at the same level as before the pressure drop [17].

- Delayed cooling under the spinneret with a hot shroud (Fig. 3.5) or by blowing hot gas to the filament: This avoids the risk of too fast cooling of the filament surface and too high preorientation. This will result in a lower take-up tension and lower pre-orientation and therefore in better drawability and higher final tenacity.
- Delayed cooling with a heater after the cooling zone [18]: Here the filament temperature is increased after the filaments pass the cold air zone with the help of a hot air stream. The yarn speed in the air quench is first reduced and increases to the full POY take-up speed after leaving the hot air tube. The final stretch takes place in the hot air tube, resulting for example for PET in a final tenacity of 35 cN/tex at 4000 m/min, which is not possible without the hot air tube until 6000 m/min (Fig. 3.6). These filaments can often be used as the final product.

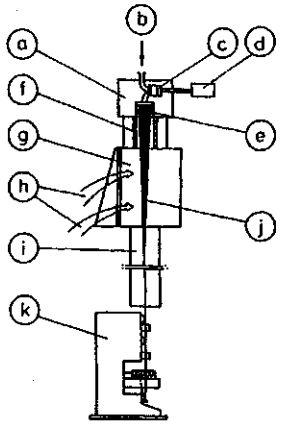

Figure 3.5
Schematic drawing of a melt spinning machine with hot shroud
a) Spinning head
b) Polymer melt
c) Spinning pump with
d) Spinning pump drive
e) Spin pack with filter and spinneret
f) Hot shroud
g) Air quench chamber
h) Quench air
i) Spinning or floor interconnection tube
j) Multifilament
k) Take-up winding machine

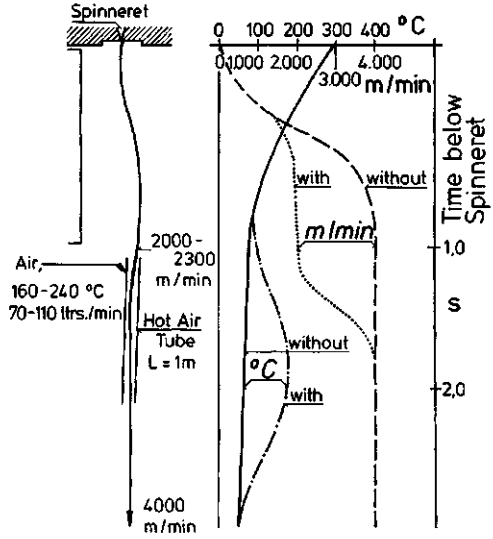

Figure 3.6
Spin draw process for PET according to ICI [18];
left: yarn path with hot air tube;
right: filament speed v and temperature T along the yarn path

3.2.2 Solution Spinning

Polymers that do not melt are usually transformed into solutions with 5...40%, mostly 20...25% concentration of solids, or into a gel with 2...7% or 40...80% solids. The solvent is regained during spinning, in the case of wet spinning through the osmotic pressure in the inside, or in the case of dry spinning through the interior steam pressure.

In wet spinning a surface layer forms after the exit from the spinneret hole into the spin bath, that then will continue to coagulate towards the inside. The solvent diffuses from the inside of the filament to the surface into the spin bath. This does not require substantial heat, but an increase in temperature of the polymer and the spin bath can significantly increase the speed of diffusion and decrease the solvent concentration in the spin bath. This will increase the polymer concentration inside the filament until solidification. The bath diffusing into the inside of the filament lets that inside coagulate as well (Fig. 3.7). If the solvent leaves faster than the spin bath enters, an underpressure is created in the filament inside, that results in a collapse of the surface into n lobed cross-sections ($n \geq 2$).

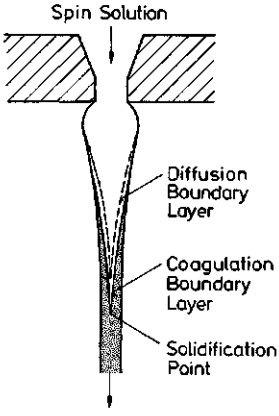

Figure 3.7
Filament formation during solution wet spinning. The shaded zone is the coagulated portion of the thread

Dry spinning works similar, except that the overpressure of the solvent in the inside is caused by an increase in temperature that is done from the outside.

A combined dry-wet spinning, also known as air-gap spinning, guides the yarn first through an air gap before submerging it into the spin bath. This air gap is usually of normal temperature, so that no relevant exchange of heat and solution happens and the yarn creation takes place like in wet spinning. In the air gap a certain amount of draft is applied, and this process is particularly suited for spinning anisotropic solutions of polyaramides, poly(ether)sulfoxide et similes or for spinning hollow filter filaments with anisotropic wall formations.

3.3 Filament Take-Up and Filament Cooling

Between the spinneret and the take-up mechanism the yarn path can be divided into three zones:

- The drawing of the melt from the spinneret hole at a melt temperature t_s and draw viscosity μ_s,
- the draw zone with filament cooling to the solidification temperature and then further to below the glass transition temperature,
- the arrival at the first solid or take-up mechanism where the temperature should be less than the glass transition temperature.

3.3.1 Filament Cooling [24]

Here the conditions according to Fig. 3.8 apply: the rheological state equation

$$\sigma(x) = \mu(x) \cdot d/dx \cdot v(x) \tag{3.6}$$

and the stability criterion

$$\sigma < \sigma_B \approx \mu(x) \quad \text{and} \quad d/dx \cdot v(x) < d/dx \cdot v(x)_{\text{critical}} \tag{3.7}$$

From this follows that a filament can be spun and taken up if it is above the critical titer (see Fig. 2.57 and 3.2). This example, especially the catenary curve, is different for every polymer. It is assumed here that σ_B is proportional to the draw viscosity μ.

This filament with almost no cross stiffness forms in a first approximation catenary [25] with the additional conditions resulting from Fig. 3.8; i.e., the degree of deviation is caused by the cross flowing quench air, the draw-down tension from the spinneret bore must be less than the melt tenacity and the final take-off tension $S_e = S_o + R + G$. Here are R = filament in the withdrawn air and G = filament weight between spinneret and take-off godet.

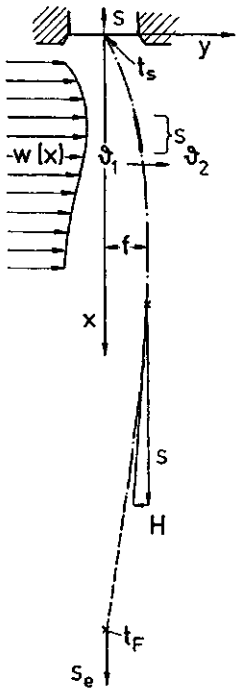

Figure 3.8
Forces along the thread path for melt spinning with cross flow air quench

For the thermal equilibrium of the filament the following is valid with the nomenclature of Fig. 3.8 [26]:

$$G_L \cdot c_L \cdot (\vartheta_2 - \vartheta_1) = G_S[c \cdot (T_S - T_F) + S] \tag{3.8}$$

S = melt heat, that somewhere in the area of the quench air $w(x)$ becomes free. For the heat transfer from the yarn to the quench air follows [27]:

$$\alpha(\Delta x, x) = \varrho dc \frac{T(x) - T(x + \Delta x)}{4\Delta x(T_m - \vartheta_m)} \tag{3.9}$$

The in part very difficult evaluation of these formulas is only possible in approximation and is explained in Fig. 3.9 with the help of some measurements:

- With the same starting temperature the filament coming from the larger spinneret hole at the same extrusion rate will cool faster due to the larger surface. At this extrusion rate, there is practically no more difference at about 500 mm below the spinneret.
- The same extrusion quantity and take-up speed result in the same finished filament diameter; the spinneret swell increases with decreasing spinneret bores.
- Spinneret swell is lower with air quench than without.
- The air quenched filament cools down faster than the filament without air quench (Fig. 3.9d and f), but without any significant difference up to about 300 mm below the spinneret.
- The heat transfer coefficients at 800 m/min take-up speed are in the average (in $W/m^2 K$):

	at 400 mm below the spinneret	at ≥ 600 mm
without air quench (b)	40 . . . 50	200
with air quench (a)	90 . . . 100	300

For other take-up speeds approximate heat transfer coefficients can be obtained by multiplication with $(W/W_0)^{0.63}$

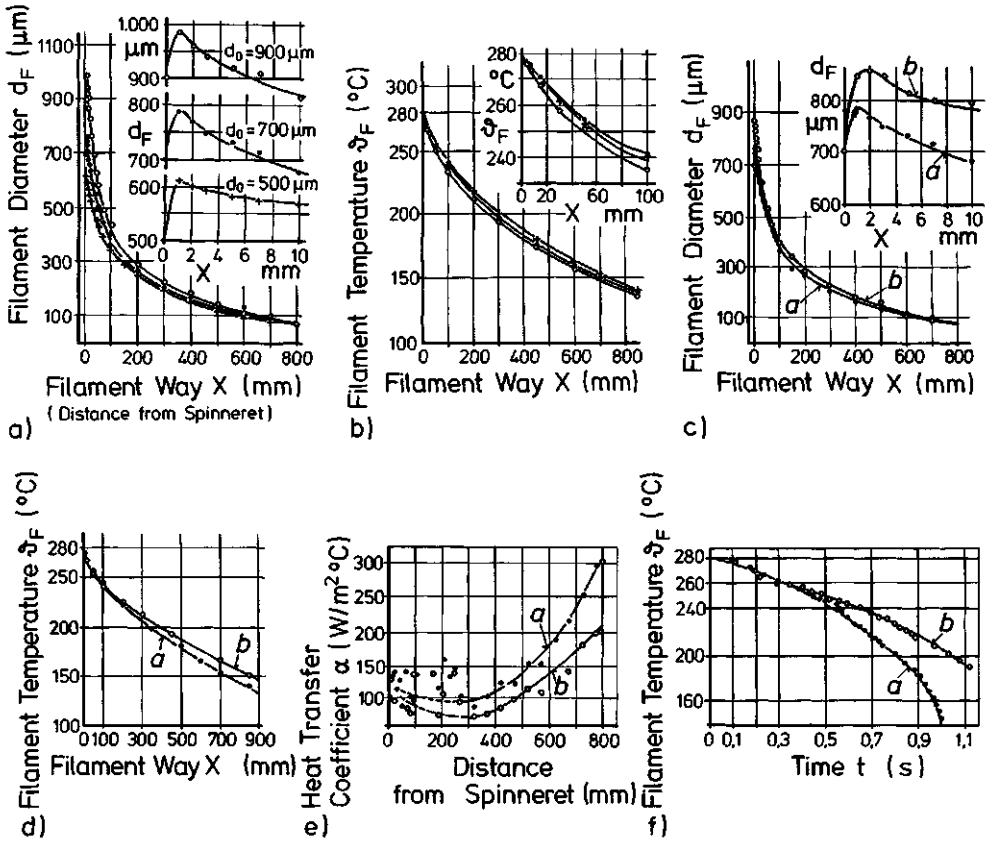

Figure 3.9 Measuring data (temperature, diameter) of a spinning and cross air quenched filament for different parameters:

a) Influence of the spinneret hole diameter on the individual filament diameter ($m = 4$ g/min, $v_e = 800$ m/min with cross flowing air)

b) Influence of the spinneret hole diameter on the filament temperature [process data as in a)]

c) Influence of the cross flowing air on the filament diameter, *a* with, *b* without cross flowing air; $m = 4.5$ g/min, $v_e = 800$ m/min, spinneret hole diameter $d_0 = 0.7$ mm

d) Influence of the cross flowing air cooling on the filament temperature [process data as in c), but $d_0 = 0.9$ mm]

e) Heat transfer coefficient α between the cooling air and the filament surface as a function of the distance from the spinneret (*a* with, *b* without air quench; $m = 4.5$ g/min, $v_e = 800$ m/min, $d_0 = 0.9$ mm

f) Filament surface temperature as a function of the time after leaving the spinneret hole [data as in e)]

From the mentioned relations the following rough calculation can be deducted:

- The necessary cold air quantity for quenching a filament bundle within a narrow space on the sides is

$$Q_L[\mathrm{Nm^3/h}] = \frac{c_F(T_S - T_F) + S}{c_L(\vartheta_2 - \vartheta_1) \cdot \gamma_L} \cdot G_F\ [\mathrm{kg/h}] \tag{3.10}$$

With:

Q_L = Air quantity per time unit in Nm^3/h
G_F = Melt or filament quantity per time unit [kg/h]
γ_L = Specific weight (density) of the air = 1.2 kg/m^3 at 20 °C
T = Polymer temperature [°C] with S for melt, F for filament
ϑ = Air temperature [°C] with 2 at the lower end and 1 at the beginning of the quench chamber
c_L = 0.25 kcal/kg K (at 20 °C, 1 bar)

The cooling air should normally have more than 80% relative humidity. The yarn temperature to be reached needs to be $T_F < T_G$ (glass transition temperature of the spin mass) minus a minor safety distance. Experience and many spinning trials show that filament breakages increase five- to ten-fold if the yarn is not below the glass transition temperature before the first contact with solid materials. If this is not possible it is necessary to take the increased number of breaks into account, e.g., for PP.

This results in a first rough formula for the necessary air quantity to cool an uninterrupted filament warp with $(T_S - T_F) \approx 235 \pm 15$ °C, a melt heat $S = 30 \ldots 55$ kcal/kg and a specific heat of 0.5 kcal/kg K:

$$Q_L \text{ in } Nm^3/h / G_F \text{ in kg/h} = 270/\Delta\vartheta_{L,\text{ permissible}} \text{ [°C]} \tag{3.11}$$

This means that with a permissible increase of the air temperature of 10 K Q_L/G_F becomes ≈27 Nm^3/kg. A more exact calculation for PA 66, PA 6, PP and PET shows significant differences, especially

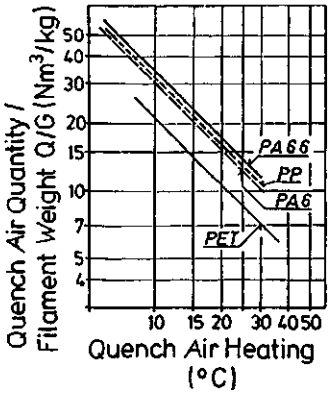

Figure 3.10
Quench air quantity requirement for cross flow air cooling depending on the permitted air temperature increase and at the outlet temperature behind the last filament row

Material	S kcal/kg	c_S kcal/kg	c_F K	Q/G $(\vartheta_2 - \vartheta_1)$	Min. quench air quantity Nm^3/kg (°C)
PA66	46.5 ± 0.4	0.66	0.66	352.5	16.8 (14 °C)
PA6	45.5 ± 0.6	0.75	0.78	312.5	14.9 (14 °C)
PET	30.7 ± 3.7	0.44	0.48	209	5.3 (20 °C)
PP	52.8 ± 2.8	0.70	0.74	324	15.4 (14 °C)

for PET (Fig. 3.10). It also needs to be considered that the glass transition temperature for PET has about 50 and for PA only about 20 K difference to the normal air temperature. Therefore it is recommended to cool the quench air for PA and possibly for PP to $< \approx 14$ °C.

- For spinning several multifilaments in one quench chamber and more extremely for monofilaments it is not possible to calculate for one filament warp, but the open spaces between the filament bundles have to be taken into account, air flowing through these open spaces does not participate in the filament cooling.

During the air quench process of the individual filament the filament heat is first dissipated to the border layer around the filament. It is then removed by the cross air. Starting with the thickness of the border layer in an even plane [39, 40] $\delta \approx 3 \cdot \sqrt{\gamma \cdot L/v}$, it is possible to deduct the cylinder diameter of the border layer for the axially moved cylinder (i.e., the filament), as shown in Fig. 3.11. Each individual filament pulls a cylinder of this average diameter downwards, respectively a filament bundle coming from the spinneret pulls a cylinder of the width of the spinneret field plus a cylinder diameter of the border layer of the outer filaments.

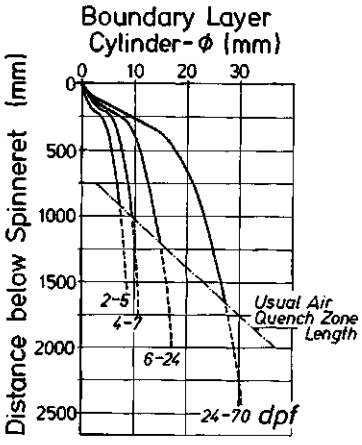

Figure 3.11
Approximate thickness of the boundary layer (D_{Gr} = boundary layer cylinder diameter) along the downward running filament as a function of the distance below the spinneret hole and the spinning titer

Spin titer in dtex p. f.	average boundary layer cylinder diameter [mm]	for yarn type	take-up speed [m/min]
0.5...1	3	PET-POY	3200...3400
2...5	3...4	PA-POY	5200...6000
4...7	5...6	PET-POY	3200...3600
6...24	10	LOY, staple fiber	1300...1750
24...70	16	carpet yarn tire yarn and technical yarn coarse titer staple fibers	500...800

Table 3.4 Filament Density Coefficient = Efficiency of Quench Air Utilization (R radius, D diameter)

Spinneret arrangement	$4 \times R$ 160	$8 \times D$ 70	$8 \times D$ 70	Radial	R 560
Quench duct width B_i [mm]	720	720	720	D 240	560
Spinneret size (width of field) [mm]	140	52	52	Warp veil	504
Spaces between hole fields [mm]	3×40	$34 \cdots 48$	45	–	–
Widths of filament border layers [mm]	8×3	16×3	16×3	–	2×3
Filament occupancy width + Border layer thickness [mm]	584 0.81	464 0.64	48 0.07	D 240 1.00	510 0.91

This allows to calculate a yarn density factor of $\varphi = \sum b/B_i \leq 1$. Only this portion of the cooling air participates in the filament cooling, or in other words, the necessary air quantity has to be increased by the factor $1/\varphi$. Table 3.4 shows some examples for this from the praxis.

This is extreme for the spinning of monofilaments, as shown by an example of 16 monofilaments from eight spinnerets with 52 mm diameter each: Here $1/\varphi$ becomes ≈ 14, i.e., the 13-fold value of the thermo-technically needed cooling air is lost ineffectively.

- For spinnerets with several rows of holes ($n > 2$) the cooling air blowing against the n^{th} row has to be cold enough to cool the filaments in this row and in all following rows sufficiently. With the average logarithmic decrement a factor

$$f = \frac{H_n}{H_1} = \frac{\ln (T_S - \vartheta_L - n \cdot \Delta\vartheta_{row})/(T_G - S - \vartheta_L - n \cdot \Delta\vartheta_{row})}{\ln (T_S - \vartheta_L)/T_G - S - \vartheta_L)} \tag{3.12}$$

can be given for the increase in the cooling distance for the nth row or for the increase in cooling air quantity to cool the farthest of the filaments in a bundle sufficiently, i.e., below the glass transition temperature (Table 3.5). Figure 3.12 shows three examples for the isotherms through a filament bundle from a large round spinneret (left), from a multi-row rectangular spinneret (middle), and from a ring spinneret (right) with inside/outside quench.

In summary the cooling requirement per quenching chamber can be calculated from

$$Q_{\text{quench chamber}} = Q_L[\text{Nm}^3/\text{h}] \cdot f/\varphi \quad [\text{Nm}^3/\text{h}] \tag{3.13}$$

Formula (3.10) for Q_L can also be used to determine the air heating per filament row or for each individual filament. Under the usual spinning conditions coarser filament titers result in an air

Table 3.5 Row Number Factor for the Air Quantity

Material	T_S [°C]	ϑ_1 [°C]	f for the number of rows of holes behind each other		
			4	7	9
PA 66	285	10	1.213	1.502	1.960
PA 6	275	10	1.216	1.525	1.991
PET	285	20	1.113	1.188	1.735
PP	265	10	1.17	1.526	1.975
		20	1.17		

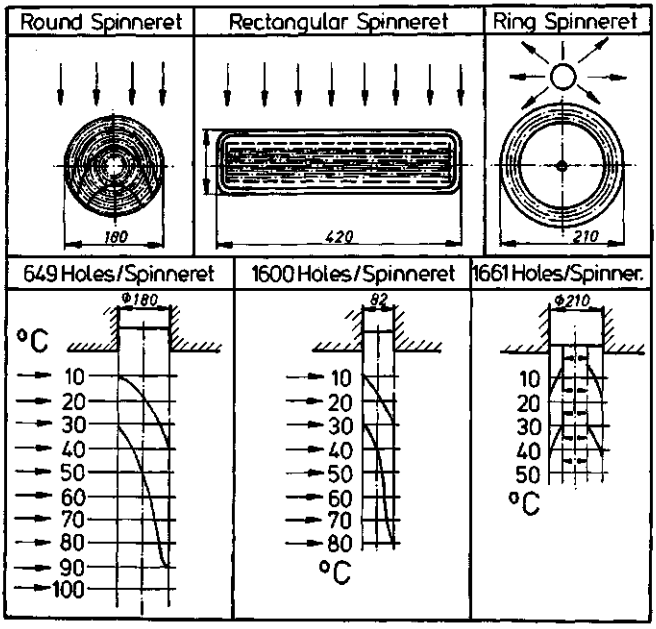

Figure 3.12
Comparison of cross and radial quench air systems; cut through the filament bundles 50 cm below the spinneret with the filament isotherms
—— 50 °C,
- - - - 70 °C,
····· 130 °C (left)
and longitudinal cut along the filament bundle center line with the filament isotherms
—— 70 °C and
- - - - 150 °C for PET spinning [29]

temperature increase of about 3.15 K/filament (e.g., carpet yarns), of about 2...2.5 K for the usual textile yarn numbers, and of 1.5...1.8 K for fine titers.

With the help of formula (3.9) it is also possible to determine the optimal cooling air velocity profile for the air quench in vertical direction (i.e., in the direction of the filament). The result is shown in Fig. 3.13 and in Table 3.6. Figure 3.13 also shows on the left how to set the air deflector sheet in the quench air supply chamber to obtain the velocity profiles on the right. It is necessary for this to have no vertical pressure exchange in the air rectifier.

The influence of the quench air profile on the Uster values is shown in Fig. 3.14 with the example of the highly sensitive PA 6: The production rate G 1.8 kg/h × chamber provides at Q/G about 0.14 m/s = 19.6 Nm^3/kg with the quench air profile A the optimum Uster value. Already at ±40% deviation from the average air velocity profile B becomes better. Similar observations can be made for spinning staple fibers with 20 kg/h × dm: Then the best profile for PET is B, and for PP it is D.

The air flow in the empty quench chamber is changed considerably by the air caught and dragged by the filaments, as can be seen in Fig. 3.15 and 3.16 in the total summation: In the upper zone, still partially liquid filament A the quench air passes through the slowly moving filament bundle. In area B the cooling air is sucked from the quench air and the surrounding air to be pressed out of the filament bundle in C

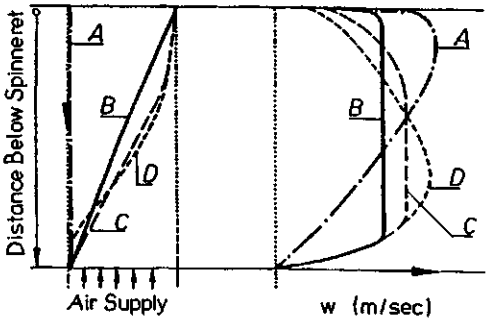

Figure 3.13
Quench air velocity profile (right) and corresponding air deflector sheet geometry in the quench air supply chamber (left, for air rectifiers with honeycombs only between fine wire meshes)

Table 3.6 Recommended Quench Air Profiles (vertical) in Dependence of the Specific Spinning Production in kg/dm Quench Duct Width

		Air supply chamber (Plenum)	Speed profile	For melt throughput [kg/h × dm]	Examples
Laminar (≤ 1.5 m/s)	A	Rectangular	Bosom profile	≤ 5	Textile, POY
	B	Diagonal	Constant(= flat)	< 10	Technical yarns, carpet yarn fiber
	C	Bottom straight Conical, top convex	Bottom constant, top Curved declining	≈ 15	Staple fiber, spunlaced, (especially PP)
	D	S-arched	Belly profile	≈ 22	Great staple capacity, yarn bundles strongly pumping downwards
Turbulent > 5 m/s)	E	Very low (≤ 50 mm high)	Constant	≲ 30	Staple compact spinning
	F	Very low (≤ 2 × 100 mm high)	Constant, counter Current	≤ 50	Very large fiber bundles, fine titers
Low turbulent (< 2 m/s)	G	Radial	Bosom profile or constant	≤ 22	Staple fiber
	H	Candle	Bosom profile or constant	≤ 22	Staple fiber

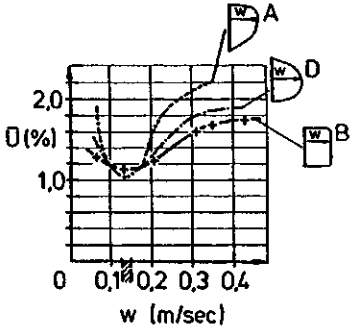

Figure 3.14
Uster values for PA 6 multifilaments depending on the quench air velocity and velocity profile (according to Figure 3.13)
(2×44 dtex, take-up speed 1000 m/min, residual draw ratio: 3.4, quench air space 0.1×1.0 m^2, $G = 1.795$ kg/h; optimum range for $Q_L = 50.4$ m^3/h, $Q_L/G = 18.7$, $v = 0.13 \ldots 0.15$ m/s, melt throughput 2.693 kg/h, in both cases is $U_{opt.} = 1.1 \pm 0.05$)

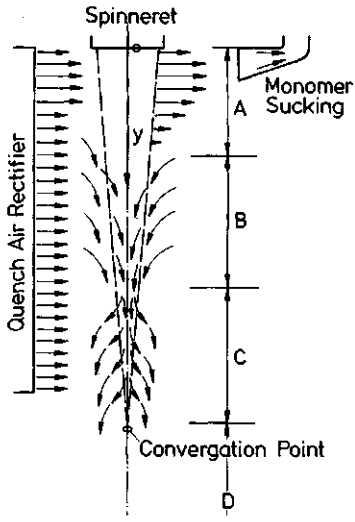

Figure 3.15
Quench air flow around and in a spinning multifilament bundle:
Zone *A*) Cross flowing passing quench air caused by low individual filament speed
Zone *B*) Quench air sucked in by a filament bundle
Zone *C*) Quench air pressed out of the filament bundle by multifilament convergence
Zone *C/D*) Convergence point made for example by an oiler pin and/or thread guide
Zone *D*) Closed filament bundle up to the take-up machine

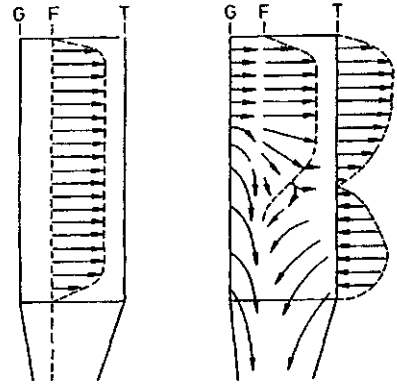

Figure 3.16
Quench air velocity distribution without (left) and with (right) downward drawn thread bundle
(planes: G = air rectifier front, F = spinneret resp. filament bundle center, T = air outlet door of the quench cabinet)

due to its convergence. The pressed out air flows due to the friction between the air and the filament bundle with the filaments out below.

The lower end of zone *A* below the upper start of the quench zone can be calculated by the following formula:

$$A_u = G \cdot [c_S(T_S - T_0) + S]/3600 \cdot b_i \cdot w \cdot c_L \cdot (\vartheta_2 - \vartheta_1) \cdot \gamma_L \qquad (3.14)$$

If $T_0 = T_G$ (=glass transition temperature) and the distance between the spinneret and the upper edge of the quench zone is added, the formula provides the lowest possible distance of the preparation godet or oiler pins from the spinneret (Table 3.7).

For the downward air flow explained in Fig. 3.15 through the floor interconnection tube there are two possibilities:

Table 3.7 Dragged Air from the Spin Filaments out of the Quench Duct to Below

Material	Titer dtex p.f. × residual drawability	Number of holes 100 mm spinneret width	Take-up speed m/min	Converging point below spinneret m	*Y* m	Spinneret space mm	Floor interconnection tube cross sections mm	Dragged air volume Nm^3/h	Average air speed downward*) m/s
PET	0.8 × 1.5	61	3200	0.57	0.3	65	350 × 87	54.7	0.5
	1.8 × 1.5	61			0.4			38.0	0.37
	2.7 × 1.5	61			0.65			30.4	0.28
	4.5 × 1.4	36	3600		1.2			25	0.24
PA 6	15 × 1.2	46	6000	4.5	2.5	190 × 50	450 × 240	1052	2.71
PET	1.75 × 3.4	500	1700	1.65	1.25	410 × 100	450 × 400	1337	2.06
PP	(2 . . . 3) × 1.8	200	4000	2.00	2.0	360 × 150	450 × 450	1960	2.69

*) only for spin tube open up and down

- the floor interconnection tube is closed at the bottom except for the filament outlet slot. With the help of air conditioning a higher air pressure is adjusted in the spinning room than in the winding room, creating in the outlet slot a downward speed of about 2 m/s. Even for a big filament outlet slot of about 200×10 mm this equals a negligible air quantity of $15\,Nm^3/h \times$ slot.

  The air sucked by the filament bundle through the floor interconnection tube downward is latest redirected above the lower flap and flows back up inside the outside tube walls. This can easily lead to turbulence and fluttering of the filaments and therefore inferior Uster values.
- If the spinning plant is only separated from the winding room by a bar grate, the quench chamber best has a uniform cross-section from top to bottom and is open on both sides. The complete amount of dragged air exits into the take-up room and returns outside the quench chamber walls back through the grate floor.

In both cases the quantity of the dragged air from the quench chamber can be determined: With y_K = distance of the filament bundle point of convergence below the spinneret and Au according to formula (3.14), the dragged air velocity in the filament bundle can be determined with $v_G = k \cdot (y_K - A_U)$. Trials determined that $k \approx 20 \pm 1$. Thus the dragged air becomes

$$Q_G = k \cdot (y_K - A_u) \cdot F_{spinneret} \cdot 3600 \quad [Nm^3/h] \tag{3.15}$$

For this Table 3.7 presents some calculated approximations that are valid within ±20% range of measurements. The average downward air velocity is only true for floor interconnection tubes that are open up and down; closed bottom floor interconnection tubes can present due to the bottle neck and the upward flow at the edge twice as high velocities. In the average this results for POY spinning of textile yarns in dragged air velocities of about 0.2 . . . 0.5 m/s, and for filament bundles, e.g., staple fibers, about 2 . . . 3 m/s for up and down open floor interconnection tubes, and for closed floor interconnection tubes twice that.

3.3.2 Take-Up Forces

- The average filament tension for a monofilament or a closed yarn [28] can be interpolated from trials to be

$$S = 1.25 \cdot 10^{-4} \sqrt{(\text{dtex})} \cdot H[\text{m}] \cdot v[\text{m/min}] \tag{3.16}$$

This results for example for a polyamide monofilament of 16.5 dtex with $v = 1000$ m/min spun from a height of $H = 4.6$ m with a residual draw of 3.4 in a filament take-up tension of about 4.3 g = 0.08 g/spin dtex.

When spinning multifilaments one has to distinguish between two areas, the upper open filament bundle between the spinneret and the thread guide or the spinning tube preparation with S_{upper} and the lower closed filament with S_{lower}. In the lower part both forces have to be added. Then follows with dtex = $n \cdot$ dtex p.f. and H = distance between spinneret and first solid point in the take-up machine:

$$S[\text{g}] = S_{upper} + S_{lower} \approx 1.25 \cdot v[\text{m/min}] \cdot 10^{-4} [\sqrt{(\text{dtex p.f.})} y_{upper} \cdot n + \sqrt{(\text{dtex})} \cdot (H - y_{upper})] \tag{3.17}$$

This results for example for $v = 3600$ m/min (POY), 165 f 32 dtex, $y_{upper} = 1.6$ m, $H = 4.6$ m: $S[\text{g}] = S_{upper} + S_{lower} = 52.3 + 17.4 = 70$ g, while for $y_{upper} = H = 4.6$ m, S becomes = 150 g. For a compact spinning plant with $H = 2.20$ m S becomes 60 g. With $H = 4.6$ m and a shortened $y_{upper} = 1.25$ m S can be reduced to about 60 g.

This can be summarized as follows:

- The height between spinneret and take-up organ should be as short as possible.
- For quench chamber preparation the oiler pin should be as close to the spinneret as possible, however the filament should be below the glass transition temperature when matching.

3.3.3 Filament Temperatures

The individual filament temperature is dependent on the distance from the spinneret.

For the air cooled filament at take-up from the spinneret downwards *Beyreuther* [37] developed the function

$$T_F = \vartheta_1 + (T_S - \vartheta_1) \cdot e^{-x/x_0} \tag{3.18}$$

with

x distance from the spinneret [m]
$x_0 = K_{S_2} \cdot \text{tex}^{0.79} \cdot D^{-0.29} \cdot v^{0.74}$
$K_{S_2} = 0.023 \quad 0.00162 \quad 0.0026$
for PA PET PP
D diameter of the spinneret hole [mm]
v take-up speed [m/min]
tex of the individual capillary

Examples for calculations according to formula (3.18) show in Fig. 3.17 that a PET-POY with 3 dtex p.f. and 3500 m/min take-up is below the glass transition temperature of about 70 °C already after 0.7 m distance.

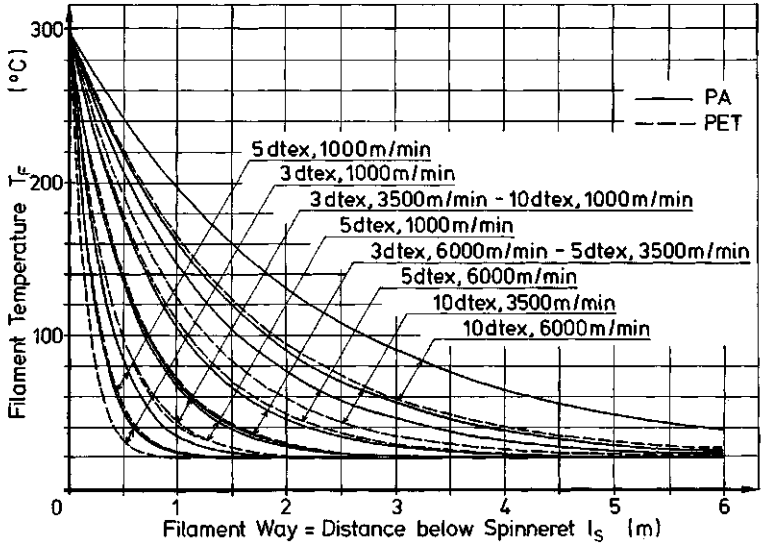

Figure 3.17
Filament temperature course T_F as a function of the filament way for melt spinning of organic high polymers [37]

By delaying the cooling of the filaments coming from the spinneret drawability and other yarn properties can be improved: Either by reducing the quench air velocity (e.g., Fig. 2.81) or by increasing the cooling air temperature [38]: With $Z = 1.11 \cdot x \cdot 10^4/v$ (m/s) · spun dtex and t_G = cooling gas temperature follows

$$t_S - 10Z + 30 \geq t_{gas} \geq t_S - 80\sqrt{(Z)} + 20 \tag{3.19}$$

for example spinneret temperature $t_S = 285$ °C, vertical distance $x = 0.2$ m, take-up speed 600 m/min = 10 m/s, 57 dpf undrawn for 16.8 dpf final titer: $Z = 3.895$. This results in $276 \geq t_G \geq 107$ °C for the quench gas temperature. An example for this is the hot shroud (see Chapter 4.7.5.3) that can improve tenacity, elongation, and fatigue strength of a PET tire yarn considerably.

The cooling of the yarn core should if possible coincide with the cooling of the yarn surface. This however depends on the inner heat conductivity of the yarn (a temperature related constant of the

material) and cannot be influenced. The optimum is reached when the inner heat supply is at least as high as the dispersion from the surface. With R = radius of the individual filament follows

$$q_i = \frac{2\pi\lambda(T_i - T_a)}{\ln(R - r_i)} \geqq q_a = \alpha \cdot d\pi(T_a - \delta) \tag{3.20}$$

This also determines the minimum cooling time for the yarn. With a given take-up speed this allows to calculate the length of the cooling zone H_1 as a function of dtex p.f. $\times v$ [m/min]. Figure 3.18 shows this dependence for the four most important melt spinning materials. For several yarn rows behind each other the value H_1 has to be multiplied with factor f from formula (3.12) to ensure that the last row is sufficiently cooled.

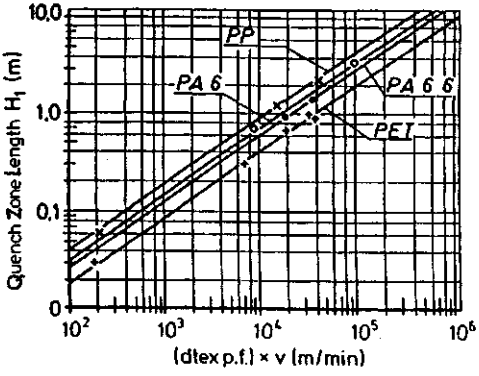

Figure 3.18
Required length of a quench air cross flow cooling zone H_1 as a function of the take-up speed × spinning titer with the material as parameter

Diagram 3.18 is also for the slit quench chambers of compact plants: For 6 dtex final or 24 dtex spin titer × 35 m/min, $v \times$ dpf becomes = 840, resulting in a cooling zone length of 0.03 m. Since the cooling air quantity only depends on the yarn throughput the air velocity becomes about 30 m/s and the total dwell time of the filament in the cooling zone is of similar magnitude as in conventional or POY spinning.

- For yarns with a minimum variation in the titer the cooling air flow has to be free of turbulences, i.e., has to be laminar or Re $\leq$ 40 (Chapter 7.10.1 ff.). For staple fibers this condition is not as important because the usual staple lengths are much shorter than the wave lengths of the filaments, normally between 20 and 60 m. Therefore it is possible to use slightly turbulent cooling air flows for filament bundles for staple fibers if the yarns can handle it due to their titer. Figure 3.19 shows the heat transfer coefficient α as a function of the Re numbers for different individual filament diameters. The conditions (3.13) and Fig. 3.12 have to be considered for this also.

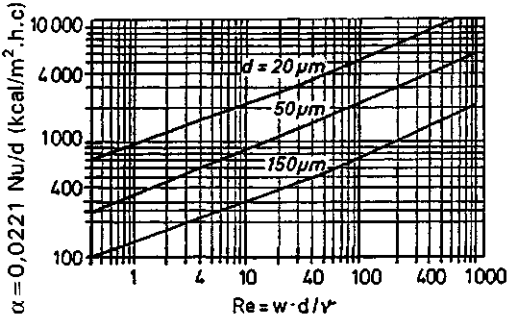

Figure 3.19
Heat transfer coefficient $\alpha = f$ (Re) ($d = 0.0221$ Nu/d; Re = $w\ d/V$) for turbulent cross flowing quench air [33] (d = individual filament diameter)

- Immediately after the (laminar) quench air leaves the rectifier, the stability conditions for the air flow in the quench chamber change as follows:

$$Re_{\text{Thread}} \leq \frac{W \cdot (x)_{\text{Thread}}\, d(x)}{\varrho} \leq 40 \ldots 80 \qquad Re_{\text{cooling chamber}} \leq \frac{W \cdot B_i}{\varrho} = 2300 \tag{3.21}$$

The first condition for the yarn is easily fulfilled, because the vertical velocity profile from the slowest velocity on the top increases steadily downwards and slowly up to the maximum value and because safely every velocity peak is avoided (1 mm filament diameter × 1 m/s air velocity = $\mathrm{Re} \approx 66$).

The second condition is more difficult to fulfill. Already 300 mm inside width of the quench chamber result in $\mathrm{Re} \approx 20{,}000$; i.e., the originally laminar flow will definitely change after some distance into full turbulence. This change starts—depending on the degree of interference at the entry—for $w \cdot L_K/\mu \approx 17{,}400$ for a smooth change from the inner edge of the rectifier to the inside wall, ≈ 7000 for 0.5 mm edge height, to ≈ 4600 for 1 mm edge height. Thus $L_K \cdot w = 0.262$ respectively 0.106 and 0.068 m^2/s. For an edge height of 0.5 mm and 0.5 m/s quench air velocity the change takes place in 0.212 m distance from the rectifier exit; for laminar cooling all filaments have to be within this area.

In general it can be concluded that the distance between the rectifier exit and the filament bundle should be as small as possible. On the other hand it should not be less than about 50 mm because then the filaments may hit against the rectifier front sieve.

- A part of the titer variations occurs because every individual filament according to Fig. 3.8 is moved backwards and forwards by a changing quench air velocity, i.e. through (isotropic) turbulence. This varies the amplitude of the degree of deviation f and at the same time the filament length between the spinneret and the take-up point. This change in length draws the filament from the melt liquid volume under the spinneret; i.e. with increasing f the filament diameter under the spinneret decreases and vice versa. Thus concludes [28]:

$$\Delta\ \text{dtex}/\text{dtex} = 2 \cdot n \cdot \Delta f / v \tag{3.22}$$

This means that with an increase in vibration frequency n and an increase in amplitude Δf the maximum titer variation also increases, but decreases with increasing take-up speed and filament tension.

Observing these deviations in the quench chamber it can be seen that the amplitudes are usually 3 ... 10 cm with a periodicity of 0.2 to about 1 s. This leads to titer variation wave lengths of 20 ... 60 m and to amplitudes that can easily reach between 0.8 and 4% that are usually caused by quench air velocity variations.

This behavior becomes especially critical when the proper frequency of the filaments is equal to the air velocity variation frequency, because this can lead to incalculably high filament and titer variations that make the yarns unusable. With a quench chamber preparation the proper frequency of the filaments can be changed by adjusting the oiler pins higher or lower.

3.4 Drawing Mechanism

The filaments wound up from spinning have a certain preorientation that is caused by the spinneret orientation and the spin draw, but they still have a certain degree of permanent elongation that will only be removed by drawing. The level depends on the material, the spinning conditions as e.g., spinning take-up speed (see Fig. 2.56), the age of the spun filaments, and other minor influences. Added to this are the drawing conditions as temperature, humidity respectively swelling, drawing speed or acceleration. Usual draw ratios for PA, PET, and PP and also for PAN are between 1 : 3.4 and 1 : 4.5, but for high tenacity yarns they can reach up to 1 : 7, for PVA approximately 1 : 10, and for gel yarns up to 1 : several hundred.

3.4.1 Drawing Process

Figure 3.20 schematically explains the drawing process in the area of the drawing zone (i.e., the neck point): This zone is about 0.3 . . . 2 mm in length for the usual titers and is almost found closely before the leaving point of the supply roll into the drawing zone. The previously randomly arranged, non-oriented chain molecules are drawn here into more or less oriented crystallites that are connected by non-oriented (amorphous) parts. The optimum temperature in the filament for this is around or just below the glass transition temperature, i.e., for dry PET above 70 °C or in water above 60 °C (see Fig. 2.62). PP with a glass transition temperature of approximately 0 °C, however, should be heated to over 60 °C. The required drawing temperature can in part be generated by the inner frictional heat from drawing (as in PA 6) or by an outer frictional heat (as by the draw pin for PA 66). The exposure time in the drawing zone is in the range of 10^{-4} s. In the case of outside heating the contact time has to be sufficient in order to reach the necessary temperature. Figure 2.59 shows an example of the sensitive reaction of the drawing zone on temperature variations.

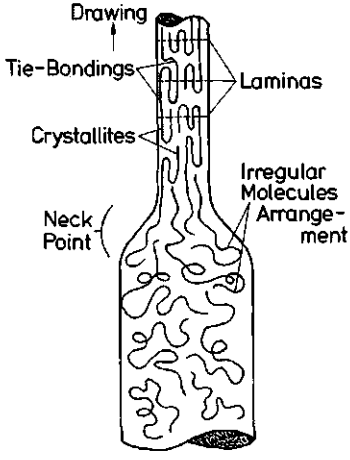

Figure 3.20
Schematic drawing of the filament neck point development (bottleneck) and formation of the molecular chain orientation in the cold drawing process [10]

The following Figs. 3.21 to 3.30 inform about the most important property changes due to drawing. Figure 3.21 shows that the breaking elongation decreases with increasing draw ratio (*B*), while the breaking tension (*D*) also increases. The metric number = 1000/tex (*A*) increases directly proportionally with the draw ratio. According to Fig. 3.22 the tenacity increases with increasing solution viscosity and with an increasing draw ratio. The elastic work capacity of the filament, however, reaches a maximum at a certain draw ratio that depends on the individual filament titer. This maximum can be described as an optimum draw ratio [42] (see Fig. 3.23).

Figure 3.24 shows the possibilities to influence the tension (tenacity)-elongation diagram by drawing: Undrawn there first is the flowing; then the filament can be elongated with little force to about 370%. As opposed to this the 3.96 fold extended filament is fully elastic up to about 0.4 N/tex ≅ 12% elongation. An explanation for this is given in Fig. 3.25, where the differential quotient $\sigma' = d\sigma/d\varepsilon$ is seen as a function of elongation. This elastic modulus is first reduced up to a small elongation to then again increase and decrease again in a third zone. An explanation for these four areas can be given as follows [9]:

- The initial modulus in area 1 is connected to the freezing temperature of the non-crystalline areas [43] and decreases initially due to the preorientation.
- The ability to recover for filaments with a low glass transition temperature is still quite significant in the second area up to the included σ_{max}; the reversible elongation of PA 6 filaments is still > 10% [44, 45].

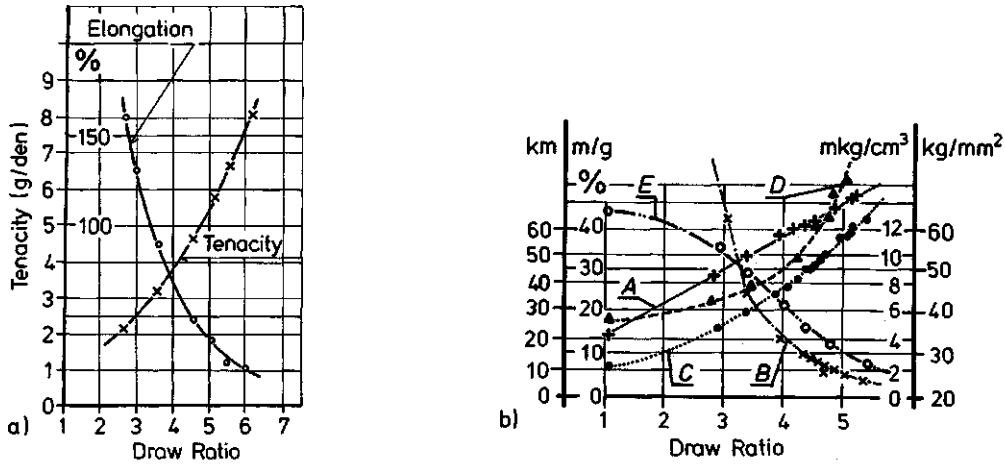

Figure 3.21 *a*) Change of tenacity and elongation of the PA 66 filament as a function of the draw ratio [41]
b) Change of tenacity, elongation, titer, total work, etc. with the draw ratio of PA 6 filaments [A: + metric count Nm), B: × breaking elongation (%), C: • breaking length (km), D: ▲ breaking tension (kg/mm^2), E: ○ total work ($m\ kg/cm^3$)]

Figure 3.22
Influence of the relative solution viscosity $\eta_{rel.}$ (measured in n-H_2SO_4) of PA 6 filaments and of the draw ratio on the tenacity

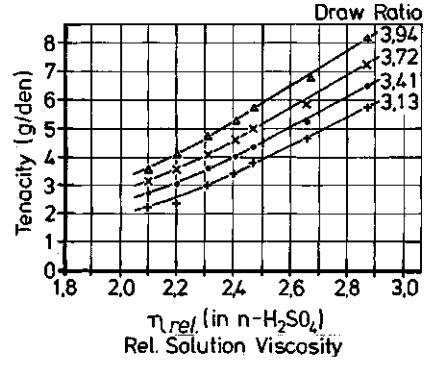

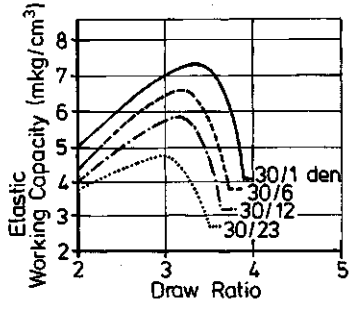

Figure 3.23
Elastic working capacity as a function of the draw ratio and of the denier per filament (according to *Boehringer* [42]); the maxima correspond to the optimum draw ratios

- in the third area further stretching is superimposed by tension reducing processes as the partial drawing of non-oriented crystallites [46, 47], creating.
- sliding processes in the fourth area [46] that make plastic deformations possible.

Figure 3.26 shows how σ and σ' can be influenced by the filament temperature in the drawing process. Also a later thermal fiber shrinkage (Fig. 3.27) influences this behavior. The drawing speed also has influence on the maximum tenacity and the maximum breaking elongation (Fig. 3.28). According to Fig. 3.29 other fibers, e.g., PAN, show similar behavior.

According to Fig. 3.30 it is also important if the filament tension and/or the tenacity is related to the original linear density or the titer achieved by drawing.

Table 3.8 refers to further connected descriptions in other chapters of this book.

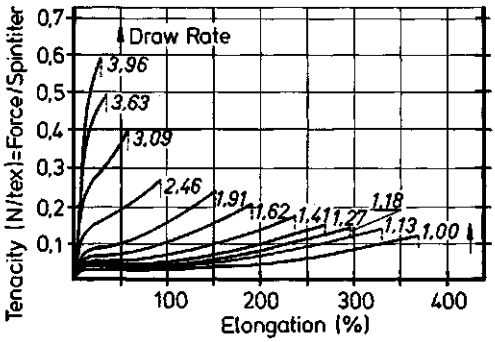

Figure 3.24
Tension-elongation diagram for differently drawn PA 6 filaments [8] (parameter: draw ratio)

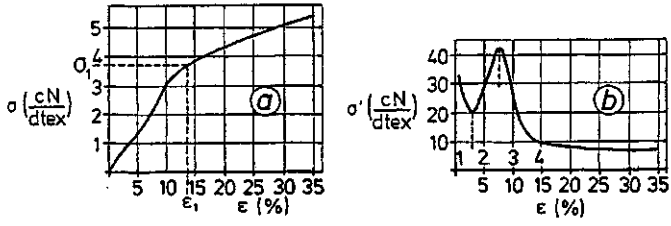

Figure 3.25
a) Tenacity-elongation diagram $\sigma(\varepsilon)$ of a PA 6 multifilament
b) $\sigma'(\varepsilon) = d\sigma(\varepsilon)/d\varepsilon$ = modulus course with elongation sections for decreasing and increasing modulus (σ_1, ε_1 = flow point; 1, 2, 3, 4 = elongation sections)

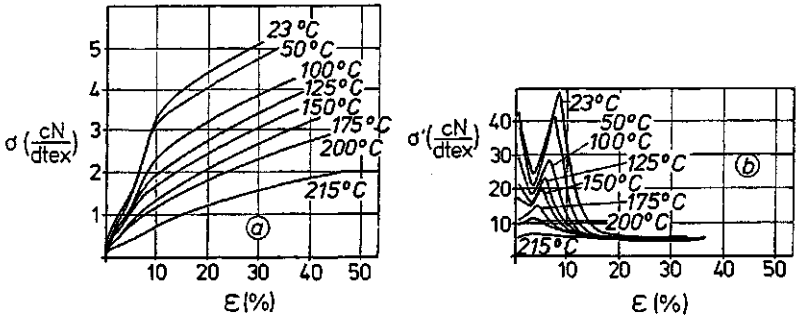

Figure 3.26 *a*) Temperature relation of the tenacity-elongation characteristics $\sigma(\varepsilon)$ of a dry PA 6 multifilament ($\dot{\varepsilon} = 1\%/s$)
b) $\sigma'(\varepsilon) = d\sigma(\varepsilon)/d\varepsilon$ (*b*)

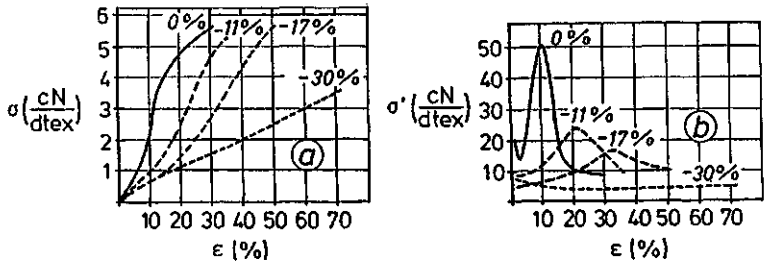

Figure 3.27 Tenacity-elongation characteristics (*a*) $\sigma(\varepsilon)$ and (*b*) $\sigma'(\varepsilon)\, d\sigma(\varepsilon)/d\varepsilon$ of differently shrunk PA 6 filaments; parameter is the thermally received shrinkage:

- 11%: in saturated steam of 105 °C
- 17%: in saturated steam of 130 °C
- 30%: in silicone oil of 185 °C

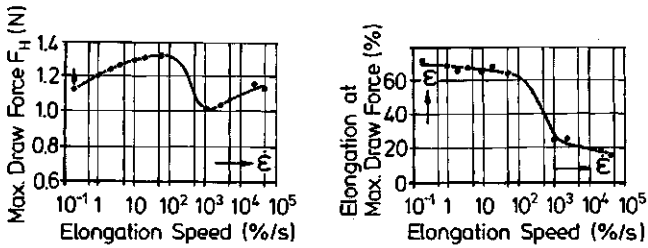

Figure 3.28 Maximum draw force F_{max} and corresponding elongation ε_{max} of a PA 6 multifilament as a function of the elongation velocity $d\varepsilon/dt = f(\varepsilon)$ according to [10]

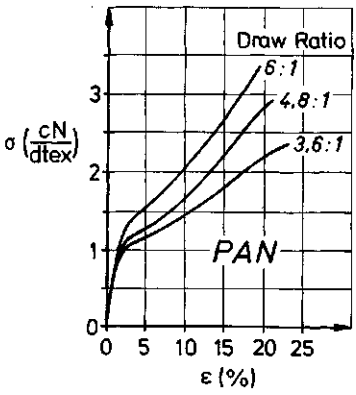

Figure 3.29 Tenacity-elongation diagrams of differently drawn PAN filaments (draw ratios 6 : 1, 4.8 : 1, 3.6 : 1

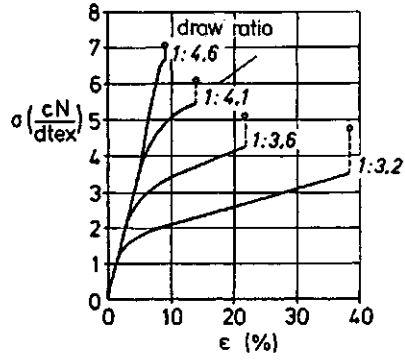

Figure 3.30 Tenacity-elongation diagrams for differently drawn PET filaments (1 : 4.6, 1 : 4.1, 1 : 3.6, 1 : 3.2) [11] (The tension is based on the starting titers; the circles ○ show the actual tension based on the actual titer.)

Table 3.8 Functional Connections of σ, ε and Other Parameters

Material	σ (ε)	Chapter	A	Chapter
PA 6	σ (ε)	2.1.43	σ_{max}, ε_{max} [% ε/s]	3.4.10
	$+ i$	3.4.6	σ^1 (ε)	
	$+ t$	3.4.9	$i(v, \eta_{rel.})$	2.1.41
PA 66	σ (ε)	2.1.53	σ_{max}, ε_{max} [i]	3.4.2
PET	σ (ε)		σ (ε, yarn type)	
	$+ v_{take\text{-}up}$	2.2.29	σ_{max}, ε_{max} [η]	2.2.31
		2.2.32		
		2.2.33		
PAN	σ (ε, i)	3.4.11	P_{draw} (i, t, medium)	2.2.30
PP	σ (ε, $v_{take\text{-}up}$)	2.3.19	σ_{max}(M)	2.3.35
PVA	σ (ε)	2.6.8	σ_{max} ($v_{take\text{-}up}$, i)	2.6.5
PTFE	σ (ε)	2.6.1		
PE-Gel	σ (ε)	2.9.9	σ, ε $(i)_{max}$	2.9.2
				2.9.3
			σ $(i)_{max}$	2.9.4
Carbon (PAN)				

3.4.2 Consequences for Drawing

For the praxis of filament or tow drawing the following can be concluded:

- By lowering the glass transition temperature the drawing force can be reduced (e.g., with the help of softening agents, oligomers, swelling agents, or residual solvents) and/or

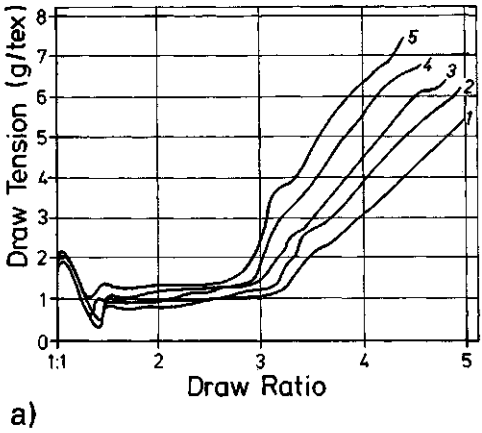

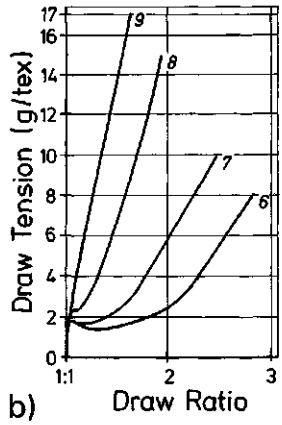

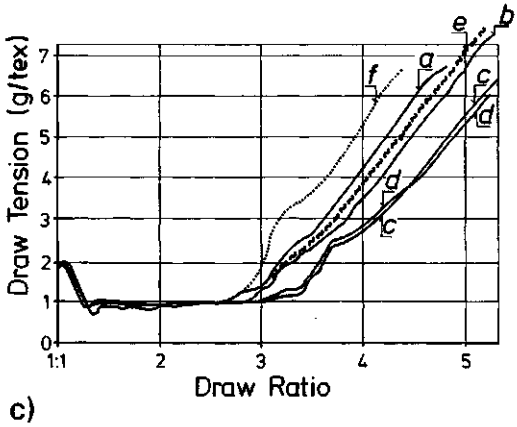

Figure 3.31 Tension-elongation diagrams for PET multifilaments spun with different take-up speeds [m/min]:

a)
- Individual titer: 1.85 tex
- Draw velocity: 500 mm/min
- Draw temperature: 70 °C
- Take-up speed [m/min]:
  1 460
  2 700
  3 850
  4 1000
  5 1150

b)
- Individual titer: 0.25 tex
- Draw velocity: 500 mm/min
- Draw temperature: 70 °C
- Take-up speed:
  6 1500
  7 2000
  8 3000
  9 4000

c)
- Individual titer: 1.85 tex
- Draw velocity: 500 mm/min
- Draw temperature: 70 °C
- Take-up speed: 460 m/min
  1 without quench duct and spin tube
  2 spin tube temperature: 70 °C
  3 spin tube temperature: 100 °C
  4 spin tube temperature: 240 °C
  5 spin tube temperature: 20 °C
  6 spin tube cooled with CO_2

- by increasing the drawing temperature. A significantly higher drawing temperature than the glass transition temperature results in filament flow and only to a reduction of the filament titer but not in an increase in tenacity.
- The stretching speed during drawing and its influence on the various parameters can hardly be generalized. For this it is better to experiment on a laboratory drawing unit with the ability to vary the distance of the drawing equipment, temperature and speed: the $\sigma(\varepsilon)$ becomes $= f\,[v_2/L\ (1 - v_1/v_2)]$ with L = distance of the draw points, v_1 = supply speed, v_2 = take-up speed with the temperature and medium as parameters.

Usual drawing zone lengths for dry cold or hot drawing of textile and industrial yarns are several decimeters, for tow for the staple production several meters, and for gel spun PE filaments 10 ... 30 m with drawing speeds of up to 2000 respectively 200 respectively 100 m/min.

At low drawing speed and temperature above the glass transition temperature the flow effect can be used to produce superfine filaments: In almost boiling water and sufficient dwell time, PET filaments can be drawn up to almost twenty times their original length with the responding titer reduction and no increase in orientation. After cooling to below glass transition temperature additional drawing can as usual increase the tenacity and decrease the elongation [51]. This process is also used for wet spun PAN filaments for carbon fiber production.

Figures 3.31 *A*, *B*, *C* allow the determination of the required draw tension as a function of the draw ratio: For the usual staple—tow spin take-up 6 ... 8 g/tex are almost never exceeded. For POY spun yarns 15 ... 18 g/tex can be reached. A practical conclusion is that for the power calculation of the drawing drive for PET and for PA, PP, or PAN filaments draw forces of 20 g/tex are always sufficient.

3.5 Twisting

By twisting the individual filaments in a multifilament yarn the filaments stay together better and also change their appearance. Therefore monofilaments are also twisted. If the yarn runs axial onto a rotating bobbin or from the bobbin, the twist density becomes

$$\text{twist turns} = n[\text{t/m}] = \text{Spindle rpm/yarn speed [m/min]} \tag{3.23}$$

The twist direction in the yarn is distinguished as S or Z twist (Fig. 3.32). Z-twisted yarns are more common; exceptions are sewing threads in S-twist and tire cord that is created by plying several twisted yarns—usually into the opposite direction. Typical twist turns for yarns from draw twist pirns are 10 ... 20 t/m, for weaving and warp knitting yarns 160 ... 240 t/m, for cord yarns 300 ... 500 t/m, and for crepe yarns depending on the titer up to 3600 t/m. For modern subsequent processing twisting is often replaced by air tangling and/or by slashing.

There are several different processes for twisting:

- Ring twisting (Fig. 4.237 left and 4.248, = down twist): Each yarn runs from a supply bobbin or from a warp beam via a supply roll through a pig tail yarn guide into the twisting balloon and then

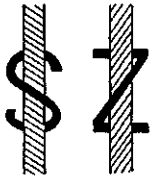

Figure 3.32
Definition of the twist direction (S respectively Z)

through a round running traveler tangentially onto the bobbin. The yarn tension is set by the selection of traveler and the spindle speed and so is the twist hardness.

- Up-twisting (Fig. 3.33): The yarn is tangentially taken off from the bobbin into a balloon and wound through a pig tail yarn guide axial onto a usually friction driven take-up bobbin. Yarn tension is only created through the yarn balloon and is therefore quite low [41], resulting in a soft twist.

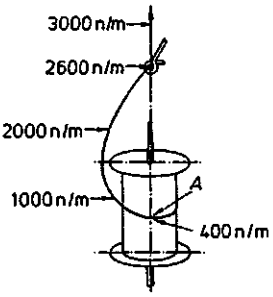

Figure 3.33
Take-up twist spindle with an example for the twist distribution of the drawn off and twisted filament

- Two-for-One-twisting (Fig. 3.34): The yarn is taken-up over the bobbin edge upwards and then led through the bobbin axis downwards, from there to the outside and runs over a detensioning ring into the yarn balloon, then through a pig tail yarn guide (*4*) to take-up. This yarn way doubles the twist: $n = 2$ t/revolution. The yarn tension is determined by the balloon, resulting in a soft twist.
- Not used for synthetic yarns is the wing twisting (yarn runs towards the bobbin over a rotating wing) and the bell twisting (yarn runs towards the bobbin over the edge of a bell) and the "Three-for-One Twisting" with a counter driven inner take-off bobbin.

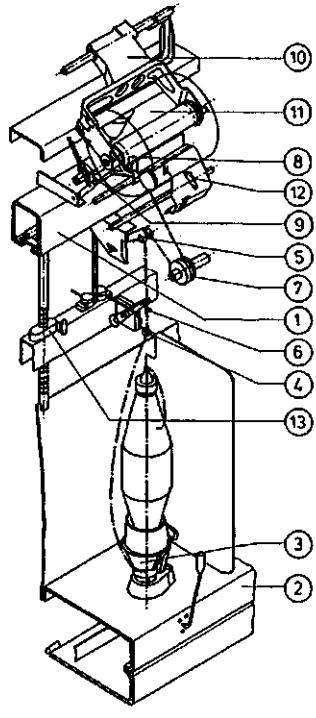

Figure 3.34
Two-for-one twist spindle with a thread path up to take-up winding [56]

1	Machine frame	*8*	Traverse guide
2	Spindle support beam	*9*	Take-up friction drum
3	Two-for-one spindle with pirn	*10*	Swivel bobbin support
4	Balloon thread guide	*11*	Take-up bobbin
5	Guide roll	*12*	Yarn reserve
6	Thread sensor (stop motion sensor)	*13*	Balloon height adjustment
7	Pre-take-up roll		

- The direct cord twisting system (Fig. 3.35): Starting point are two twisted bobbins (*1* and *a*). The first yarn runs from a supply roll through the hole in the other bobbin to the twist point (*5*), where this one twists around the first yarn. By choosing S and Z and the two yarn tensions correctly, a cord yarn is created in point (*5*) that is hardened between (*7*) and (*11*) by high tension drawing and then wound.

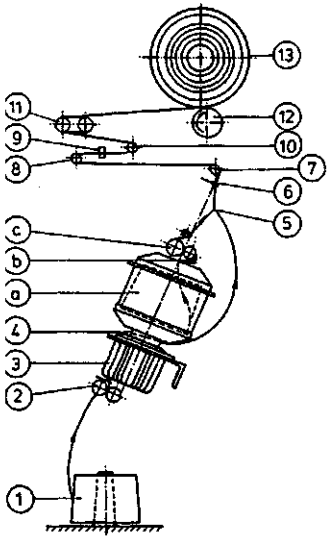

Figure 3.35
Schematic drawing of the direct cord machine (system AKU, construction: Barmag [56])

1	First take-off bobbin	*5*	(combining) twist point
2	Supply roll	*6*	Yarn guide
3	Twist motor	*7, 8, 10*	Yarn guide rolls
4	Centrifugal disc	*9*	Stop motion sensor
a	Second take-off bobbin	*11*	Take-up duo
b	Thread guide roll	*12*	Friction drum
c	Second supply roll	*13*	Take-up bobbin

Except for cord twist yarn the yarn tension for textile twisting of PET yarns should be between 0.7 and 2.7 g/tex, and for PA yarns corresponding to their lower elastic modulus somewhat lower.

Figures 3.36 are diagrams to determine the yarn tensions in up-twisting and two-for-one twisting (*A*, *B*) and in ring twisting in the balloon between the traveler and the bobbin (*C*, *D*).

By tilting the individual filaments with respect to the yarn axis twisting changes yarn properties; Figure 3.37 shows an example of a dependence from the twist angle (between yarn axis and individual filament) α.

3.6 False Twist Texturing

The natural fibers wool and cotton are crimped. To achieve a similar effect and possibly that of staple yarns many methods have been developed (Chapter 4.12), of which false twist texturing is today the most used. If it caused the bulk and yarn elasticity remain too high, they can be heat-set in a second step under partial drawing: a set yarn is created.

3.6.1 Principle

Until about 1956 a multi-step—twist heatset—untwist process was used [57] (Fig. 4.255A), that was replaced 1957/58 by a previously known continuous process [58]. Here a stationary or a moving yarn is twisted between two fix and not turning delivery points *a* and *c*, for example into Z direction. The result for the portion between *a* and *b* is S twist, and for the portion between *b* and *c* it is Z twist, i.e., the sum cancels out to zero twist (Fig. 3.38). For moving yarns the S twist starts at *a* and stays constant up to the

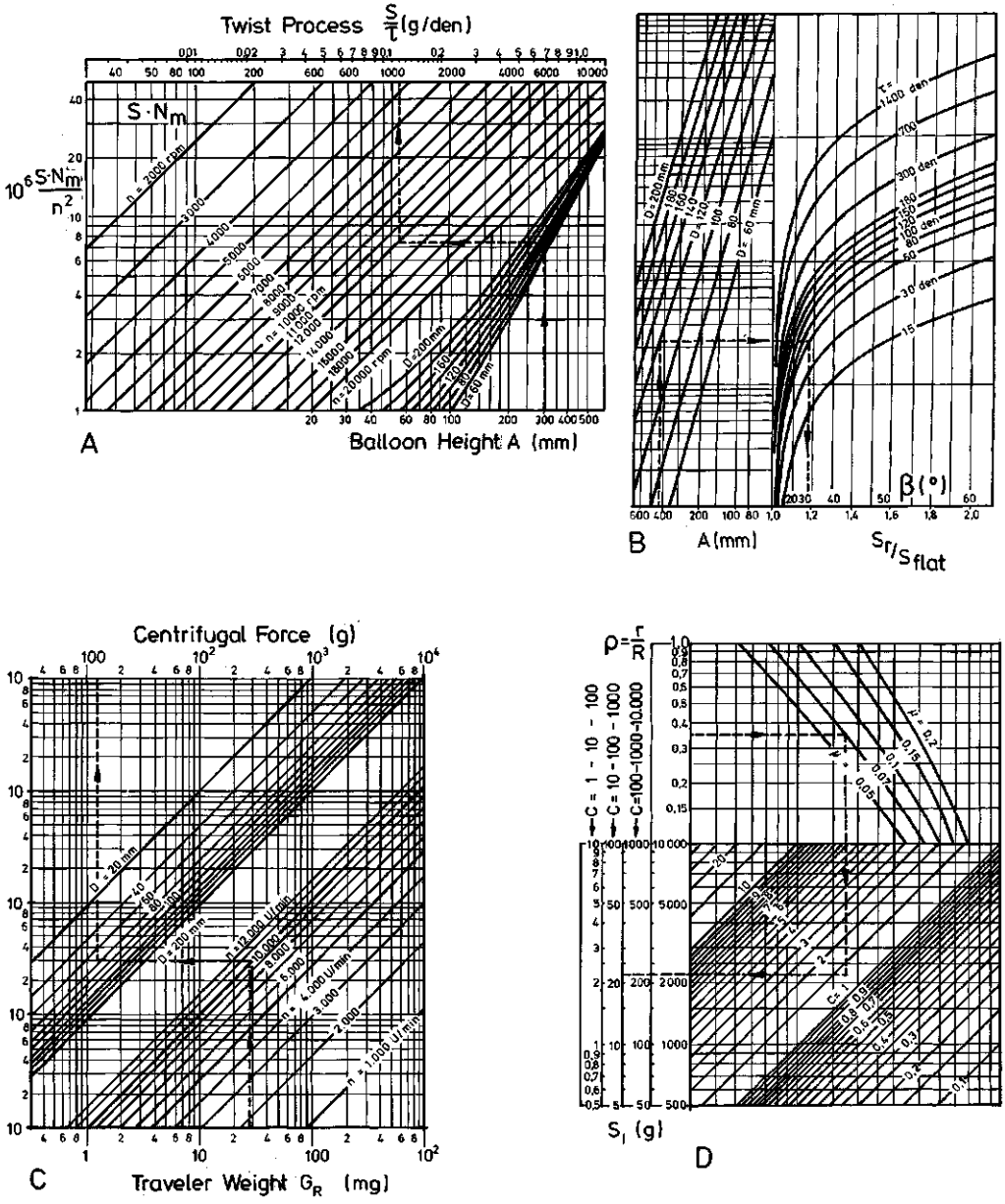

Figure 3.36 Diagram for the determination of the yarn tension S/τ during twisting

A) For take-up twisting as a function of the balloon height A, the bobbin diameter D, the spindle rpm n, in g/den without air resistance

B) Factor of increase for the balloon tension according to A by air resistance

C) Centrifugal force of the traveler C as auxiliary and as a function of the traveler weight G_R, spindle rpm n, and ring diameter D

D) Yarn tension between the traveler and the cops for ring twisting (down twisting) as a function of the ratio of cops diameter (r, d) to the ring diameter (R, D), of the friction coefficient μ for the traveler (for oil lubricated rings $\mu = 0.18$ for 15 m/s, reduced to 0.08 for 40 m/s and 0.06 for 60 m/s) and of the centrifugal force C [g] [53]

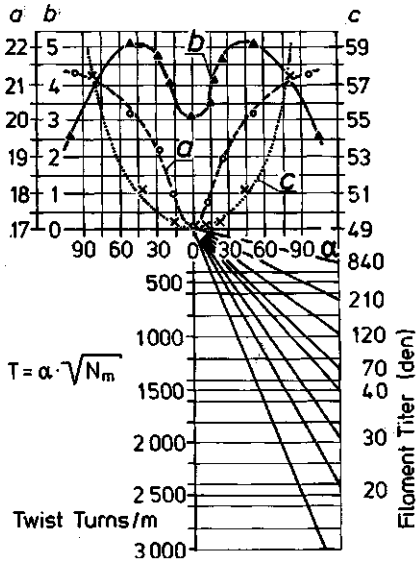

Figure 3.37
Tenacity, elongation, and twist shortage of a PA 6 multifilament in dependence of the twist (t/m) and the titer (den)
a) Elongation (%)
b) Twist shortage (%)
c) Breaking length (km)

twist element at *b* and then it dissolves. If the yarn is heat-set in the area between *a–b* in the highly twisted state, i.e., heated sufficiently and then cooled again, the twist will be removed behind *b*, but the crimp caused by the twist remains. Additional partial drawing and heat setting after *c* can partially remove a portion of the bulk and elasticity again.

Table 3.9 presents the formulas and titer depending values for the recommended twist values in point *b* in Fig. 3.38 (according to *Heberlein* [2] and Barmag by interpolation of the trials, according to *Fourné* [59] by mathematical spring optimization. In praxis the actual values for yarn, machines, and false twist spindle should be determined case by case near these table values by experimentation.

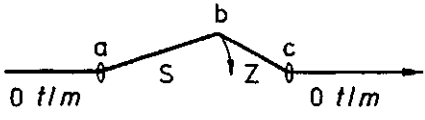

Figure 3.38 False twist principle

Table 3.9 False Twist Values [t/m]

According to titer (dtex)	22	67	167	220	t/m according to formula	Process
Heberlein [2]	4230	3080	2106	1865	$800 + 305\,560/(67 + \text{dtex})$	Real twist
Fourné [59]	3658	2951	2123	1891	$30\,180/(1 + 16{,}7/\text{dtex})\sqrt{\text{dtex}}$	Real twist
Barmag	5165	3457	2221	1940	$800 + 305\,560/(48 + \text{dtex})$	False twist

Lünenschloß [60] found about 3500 m/min to be an optimum spin take-up speed for textile PET yarns for draw texturing; other trials between 1750 and 5500 m/min [61] confirmed this. This speed resulted for the textured yarns in the best bulk coefficients ($KD = 87 \ldots 90\%$), not yet damaged tenacity, and sufficiently low breaking elongation. The trial results were tested and valid for 40 f 17 to 165 f 52 dtex, spin draw about 150 ... 350 and spinneret hole diameter 0.20 respectively 0.25 mm. Similar values are true for PP false twist, see Fig. 2.84 and Table 2.19.

3.6.2 Influence of the Filament Way Profile

The optimum filament way geometry is controversial. Figure 3.39 shows the so far used heater–cooler arrangements for the high twist area and for the set area behind the false twist spindle. The results thus far can be summarized as follows:

- The filament tension up to 620 m/min yarn speed for all arrangements is about 30 cN; for *1* and *2* it increases up to 1100 m/min to about 40 cN with a possible increase in filament breakages. For *3* the yarn runs rather smoothly at 900 m/min; $\geq$ 1000 m/min result in increasing ballooning, that also starts here for *4* and *5* and additionally causes increased yarn tension variations.
- Increasing the heater temperature from 190 ... 200 °C to about 240 °C reduces the yarn tension in *1* to *3* from 36 to 30 g, running smoothly. The yarn course according to *4* is unstable for $\geq$ 900 m/min for all temperatures.
- An increase in the draw ratio from 1.50 to 1.58 increases the yarn tension from about 30 to about 40 g and results in an unstable course for *4* and *5*.
- An increase in the texturing speed from 600 to 1100 m/min reduces the achieved yarn twist with the same spindle from 3600 to about 3000 t/m without any other effects.
- For a *D/Y* ratio of 1.85 ... 2.05 hard friction discs achieve good twist transfer and no notable changes in the crimp coefficients.
- For > 200 ... 210 °C heater temperature the tenacity and the breaking strength of PET decrease significantly.
- For *1* to *3* and > 900 m/min and for *4* and *5* with > 800 m/min the yarn breaks increase significantly as they do at heater temperatures of > 220 ... 230 °C. With an increasing *D/Y* ratio the yarn breaks decrease for *1* to *3*, but remain constant for *4* and *5*.

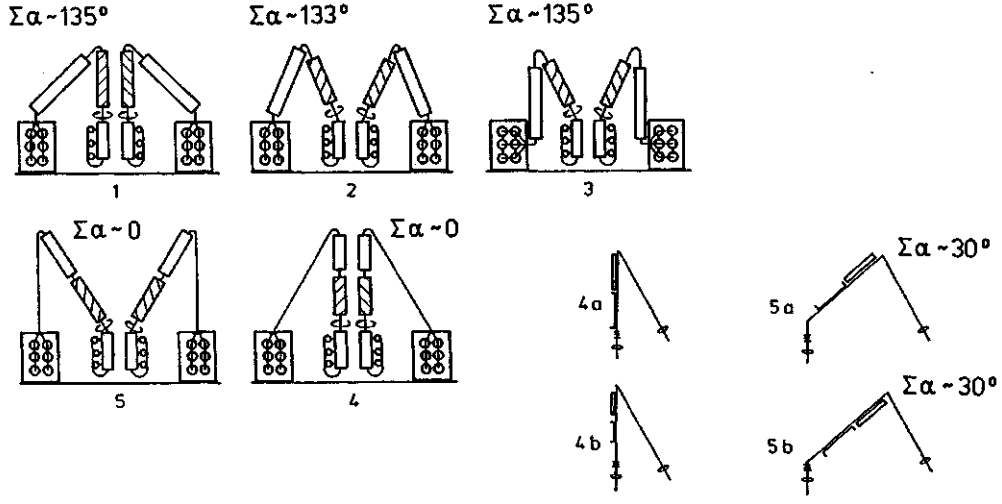

Figure 3.39 Arrangement of heater plates and coolers in false twist texturing machines

No.	Barmag	Giudici	ICB-ARCT	Murata	Rieter-Scragg	RPR	Sum of angles
1	FK6-L	IG-20					≈ 135
2	FK6-M						135
3	FK6-U			333-II/336	SDS/BCS	35 D	135
4	FK6-S						0
5	FK6-V	IG-20	FTFB-E 2	335	SDS/BCS	35 D	0 ··· 30

Heater lengths: 1 to 5a: 2.40 m, 4b and 5b: 1.80 m
Cooling groove lengths: 1 to 5a: 2.00 m, 4b and 5b: 1.50 m
a, b: Different plate or groove arrangements respectively lengths

- Higher texturing yarn speeds result in higher abrasion (monomers, oligomers, finish preparation) and require more frequent machine cleanings (residue quantity about 5 mg/h × spindle at 600 m/min to 10 . . . 20 mg/h × spindle at 1100 m/min).

Even though there are machines with all five yarn way geometries according to Fig. 3.39, the emphasis is on the arrangements *3* and *5*. Number *5* with heater and cooler in straight sequence is especially advantageous for fine titers and for PA 66 because the yarn angle is minimized. However the higher yarn speeds result in longer heaters and coolers and thus higher machines, causing limits due to the increasing difficulties in operation. For PET arrangements *2* or *3* are preferred, and only for fine titer PA 66 yarns number *5* is preferred.

A further reduction in height [68] with an additional pre-heating godet was not widely accepted. According to [73] strongly curved heater and cooler plates have higher heat transfer coefficients and allow shorter heaters and coolers and lower machine construction heights.

Filament Heating and Cooling

Even though the yarn appears to touch the slightly curved heating rail, the high twist speed creates a boundary layer around it, so that the heat transfer is difficult to measure [69]. Figure 3.40 shows measured heating curves for yarn speeds between 200 and 750 m/min and Fig. 3.41 the resulting necessary heater lengths as a function of yarn speed with material and titer as parameters [70]. The achieved yarn temperature remains about 10 K under the heater temperature [71] and can be measured in ms; this is enough for sufficient heat setting (see Fig. 3.70).

The necessary yarn cooling follows Fig. 3.42 and can be done in air (risk of ballooning) or over an air or water cooled rail. If possible the temperature here should reach below the glass transition temperature.

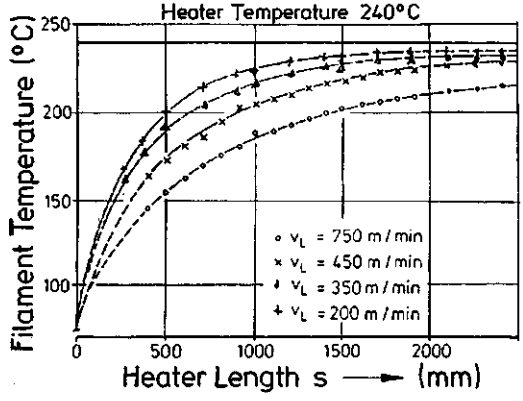

Figure 3.40
Filament temperature profile T_F in the texturing zone as a function of the texturing speed (yarn speed) with 240 °C heater temperature; v_L (m/min): +200, ρ 350, × 450, ○ 750)

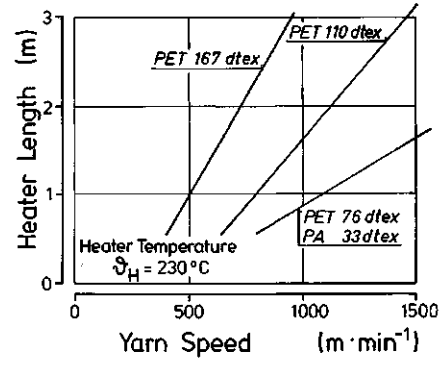

Figure 3.41
Required heater length as a function of the material, titer, and yarn speed (heater temperature $\vartheta_H = 230$ °C)

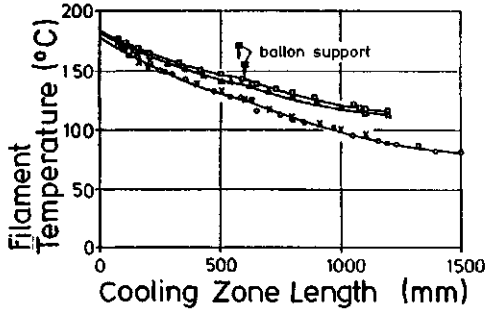

Figure 3.42
The yarn surface temperature T_F during texturing in the cooling zone for friction texturing as a function of the length of the cooling zone and the yarn speed ($v_L = 400$ m/min; cooling groove length: ■ 950 mm, × 1200 mm, ○ 1500 mm, $\Delta v_L = 500$ m/min, □ $v_L = 600$ m/min)

In machines built since 1988 the first heater is usually 1.5 . . . 2.5 m long, the second (for heat set yarns) between 1 and 1.6 m, and the cooling plates between 0.6 and 2.5 m. Table 3.10 shows the installation data including the machine power for one producer [73]. The originally resistor heated and thermistor controlled heating plates do no longer suffice today's eveness requirements, so that all companies use Dow vapor condensate heated systems (Fig. 4.262). To compensate higher temperatures for the heater length has a negative influence on the yarn quality. At present developments are underway, however, to shorten heater lengths to about 500 mm with convective heaters of up to 600 °C [108].

Table 3.10 Installed Heater, Cooler, and Power [18]

Barmag type	v_{max} mechanical m/min	Length of plates m			Power Consumption W/filament**			
		L_1	L_{cooler}	L_2	W_1	W_K	W_2	Antrieb
Fk6—80	1200	2.5	2.1	1.6	222	W	56	240
Fk6—900	900	2.5	2.1	1.46	134	W	42	208
Fk6—700	700	2.0	1.5	1.3	139	L	42	185
Fk4 S*)	400	1.5	0.3	0.8	62.5	L	62.5	134
Fu4 *)	185	1.0	0.3	0.3	62.5	L	62.5	107

*) discontinued; **) installed power up to twice; W = water, L = air

The influence of spinning and texturing speeds for PA 66 filaments with constant heater length were investigated according to Fig. 3.43: For 44 f 13 dtex an increase in spinning speed from 800 to 1200 m/min has no influence on the texturing speed if the heater temperature is increased from 213 to 237 °C to achieve a yarn temperature of 190 °C. Already at 78 f 17 dtex the heater and temperature increase are not sufficient any more; already at 400 m/min the desired twist is not achieved until about 1000 mm yarn length, so that the remaining heat setting time does not suffice (Fig. 3.44).

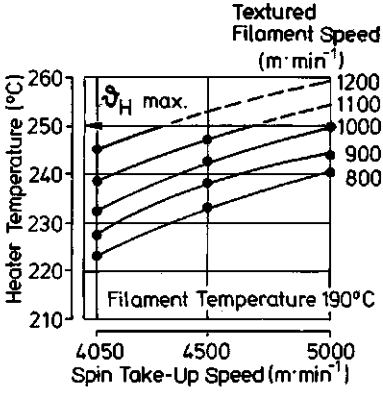

Figure 3.43 Influence of the spin take-up and texturing speed on the achievement of a constant filament temperature at the heater zone end ($\vartheta_{FH} = 190\,°C$) and the necessary heater temperature variation

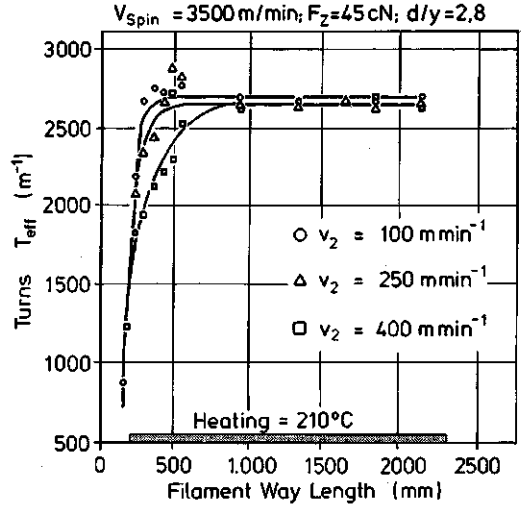

Figure 3.44 Influence of the texturing speed v_L on the actual twist density of the filament in the heater groove (v_L [m/min]: ○ 100, △ 250, □ 400; spin take-up speed 3500 m/min, take-up tension 45 cN, $D/Y = 2.8$)

Here it becomes obvious that a pin spindle transfers the twist more effectively into the yarn than a friction aggregate. A change of $D/Y = 1.8$ to 2.2 has no effect.

Trials determined the twist loss by due to the directional change in arrangement *2* in Fig. 3.39: The upper 320° turn resulted depending on the titer and material in a twist loss of 4.5 ... 5.5%; the lower turn of 30° right in front of the spindle resulted in 2 ... 2.5% loss.

From the production formula, the heat transfer through a rotating cylinder to the inside, and the necessary heat to achieve from a starting temperature (*1*) to a final temperature (*2*), it is possible to calculate the heat transfer coefficient between heating or cooling plates and the yarn surface (under consideration of the packing density of the yarn):

$$\alpha = \frac{5 \cdot \text{dtex} \cdot \text{m/min} \cdot c}{10^6 \cdot D\,(\text{m}) \cdot \pi \cdot L} \ln \frac{\vartheta - T_1}{\vartheta - T_2} [\text{kcal/m}^2\,\text{h K}] \tag{3.24}$$

The result for PET yarn with $T_1 = 20\,°\text{C}$, $T_2 = 220\,°\text{C}$, the heater temperature $= 240\,°\text{C}$ is an $\alpha \approx 0.025 \cdot \sqrt{(\text{dtex})} \cdot [\text{m/min}]/\text{L}[\text{m}]$ and thus for example for 167 dtex, $L = 2.5$ m and 1000 m/min about 130 kcal/m^2 h K.

3.7 Bobbin Construction

Basically two types of winding can be distinguished:

- Precision Winding (Fig. 3.45a)
  Traverse rpm and bobbin rpm are in a fixed ratio to each other (e.g., by gears or timing belts), thus the number of traverse motions per bobbin rotation stays constant.

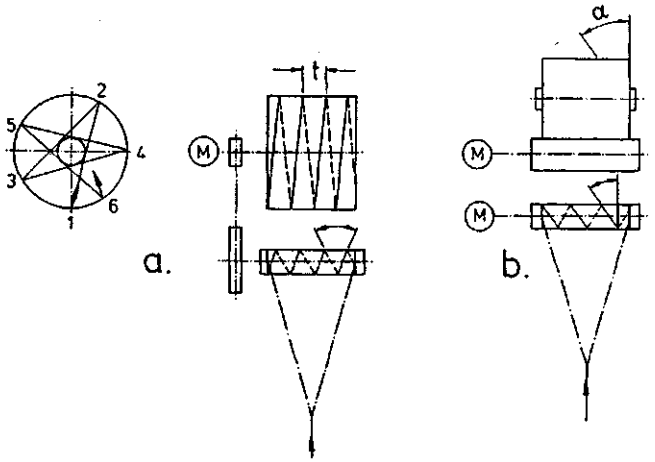

Figure 3.45
a) Precision winding: common drive for the winding bobbin and the traverse with a constant ratio between them
b) Wild traverse winding—with friction drive for the bobbin (random winding): Two independent drives, one for the friction drum and the second for the traverse motion system

- Wild Traverse Winding (Fig. 3.45b)
  Bobbin and friction drum have the same surface speed; traverse motion and friction drum are coupled, thus the angle of the yarnway on the bobbin can remain constant.

The advantages (+) and disadvantages (−) of these types of winding are:
Precision Winding:

+ no wild winding
+ good take-off properties

– bobbin construction not very stable*
– expensive winding machine

Wild Traverse Winding (Random Winding):

+ bobbin built-up stable for limited bobbin diameters
+ constant packing density
+ inexpensive winding machine
– partial wild winding*
– in part not so good take-off properties**

* can be improved with 1 bobbin revolution = $n/2$ + small irrational number with $n \geq 6$.
** can be improved by visual disturbance.

The visual disturbance is created by "wobbling": The traverse speed is periodically disturbed up to ±5% with a period of 0.5 . . . 3 s, e.g., in the shape of a saw tooth or the like (Fig. 3.46) (e.g., by changing the rpm in the traverse motion shaft), which changes the yarn angle to the bobbin: The yarn layers are less parallel as they are without the wobbling.

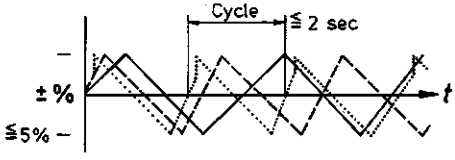

Figure 3.46
Typical wobble profiles for friction drive

To use the advantages of both systems and mostly avoid their disadvantages, it is possible to mix both systems with microprocessor control [62, 75, 76] in dependence of time or similar.

Due to the reversing of the yarn at the edge of the bobbin and the resulting increase in mass because of the decreasing angle, hard bobbin edges can occur. They can be avoided by "breathing" (Fig. 3.47). Here the turning point is moved in the axis direction periodically by $\leq \pm 2$ mm (periods of up to several minutes). Another process uses a sudden turn and knock of the traverse yarn guide [77].

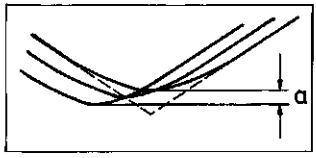

Figure 3.47
For the definition of breathing *a* in the traverse motion system

The step precision wind is formed by a sequence of constantly decreasing traverse ratios of the individual precision winds [78]. The number of the take-off tension peaks, especially for textured yarns, is reduced here to less than 1/3 and the bobbin hardness is more even than with wild traverse winding (Chapter 4.9.5.6, Fig. 4.227).

For all types of winding the following is true [76]:

$$z_W = b/n \cdot d \cdot \tan \alpha \tag{3.25}$$

z_W is the number of winds in the winding width, b, d is the bobbin and cartridge diameter, α is the yarn angle. For flat yarns α should be $\alpha \geq 7°$ to avoid too many overthrowing ends of the yarn, i.e., yarns that slide off at the front of the package.

In addition to the cylindrical cross bobbin (*zK* in Fig. 3.48) that represents the usual spin bobbin, there is the conical cross bobbin (a), the bi-conical cross bobbin (b) and the flanged bobbin (c). The latter is only used for parallel winding of monofilaments with $> \approx 0.1$ mm diameter and for ribbons and foil yarns.

The necessary traverse motion in spin take-up winding prolongs and shortens the yarn way periodically in the traverse triangle. This variation in take-up tension migrates backwards to a point that can absorb it. This can either be the melt liquid thread part under the spinneret (e.g., in godet free

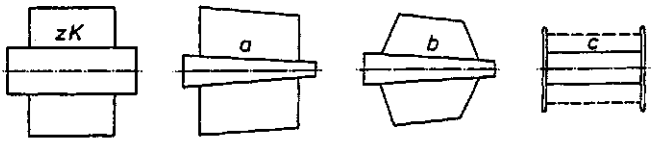

Figure 3.48
Conical cross bobbin (a), bi-conical cross bobbin (pineapple cone, (b), flanged bobbin (c) and cylindrical cross bobbin (Alexander bobbin, zK)

POY spinning), resulting there in titer variations, or it can be an intermediate godet with one or more wraps that separates the spinneret take-up tension from the winding tension. According to Fig. 3.49 for example the Uster value of a PET-POY filament can be improved from without godet (0.7%) to with $2 \times 180°$ winds on a godet (0.5%) to 7 wraps from one godet with idler roll (air supported) or one godet duo (approx. 0.3%) [78].

The most frequent reasons for bobbin construction faults are:

- wrong ratio between traverse motion and winding speed,
- wrong winding tension on the winding package (Fig. 3.50) [106]: With increasing too high winding tension the edges build up and in the center a saddle appears, then sloughed off yarns and yarn breaks. Too low tension results in a ribbon like surface and pressed out bobbin edges, then an increase in sloughed off yarns and finally loop formation, yarn breaks and wrap ups on the friction drum (Fig. 3.50).

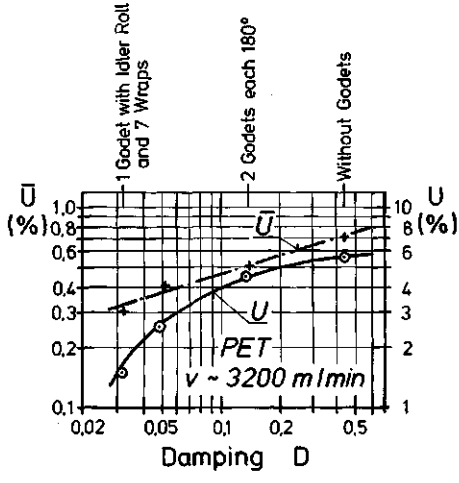

Figure 3.49
Influence of the number of wraps around godets on the filament Uster value for POY spinning of PET ($v \approx 3200$ m/min)

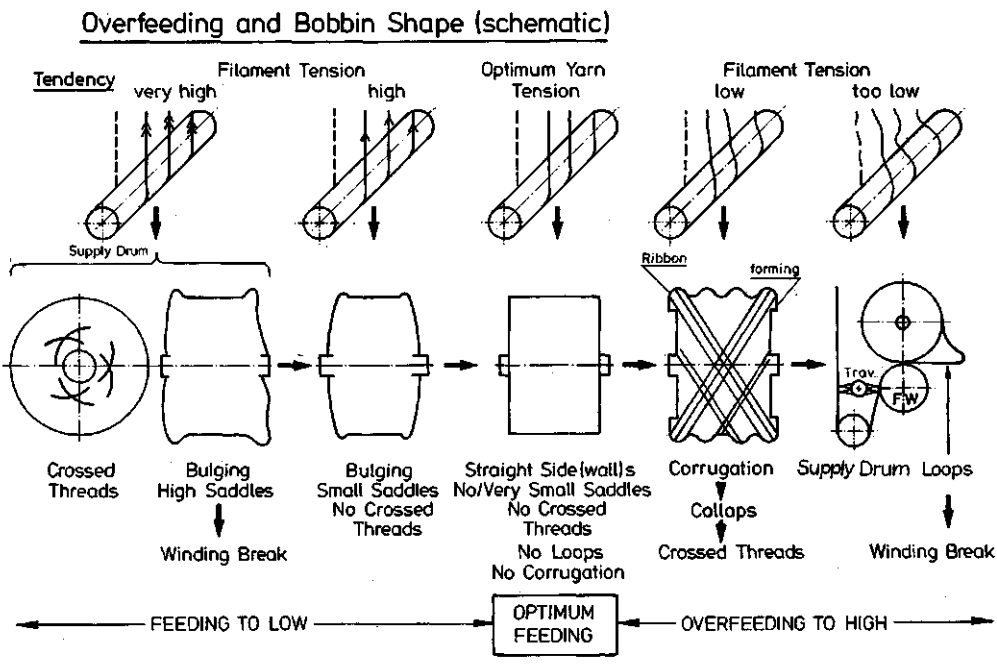

Figure 3.50 Influence of the actual winding tension on a spin cross bobbin: left: too high, middle: optimum, right: too low filament tension between the last supply drum and the bobbin

3.8 Cops Built-Up in Draw-Twisting and Cops Take-Off

In draw twisting the yarn is only wound onto copses (or pirns). The tangential entry of the yarn from the balloon occurs through a traveler that rotates around a ring (see Chapter 3.5), and the yarn is simultaneously twisted. The resulting cops form and its build-up considerably influence the take-off tension, that is desired to be constant. In turn it is dependent on the winding tension that may not exceed certain yarn specific values. For the latter the following formula was found, neglecting certain minor terms of the second order [80]. Labels as in Fig. 3.51:

$$P_t \approx \mu C/r/R + \mu\sqrt{1-(r/R)^2} \qquad \text{with } C = (G_{RL}/g)Rw^2 \tag{3.26}$$

For example with a 100 mm ring diameter and 10,000 rpm and a traveler weight of 0.024 g, $C = 145$ g and $S = 4.8$ g for 66 dtex. The friction coefficient μ for the traveler results from Fig. 3.52. Figure 3.53 shows the measured yarn tension curve that indicates the periodic variations between the winding tip at its smallest diameter and the winding base with the largest diameter. There is a strong relationship between the ratio of the winding radius and the ring radius r/R, that should not exceed 1 : 3 (Fig. 3.54). According to this the tension P_t is proportional to the traveler weight and the friction coefficient μ and proportional to the square of the spindle rpm.

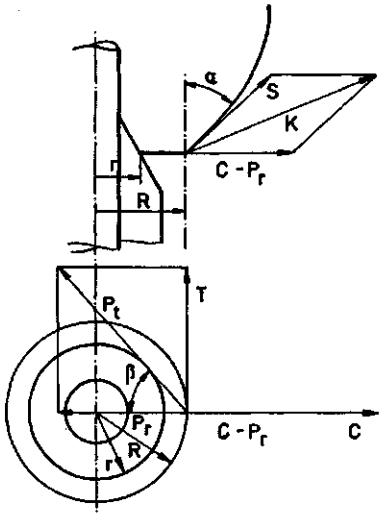

Figure 3.51
Parallelograms of forces at traveler during ring twisting between the balloon tension S and the pirn winding tension P_t

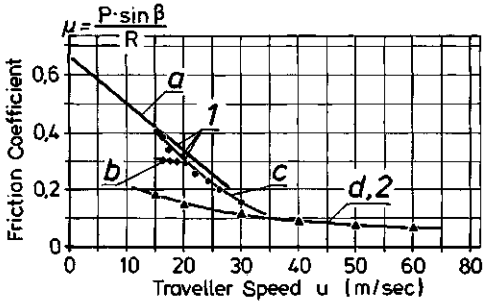

Figure 3.52 Traveler friction coefficients μ ($=P \sin \beta / R$) as a function of the traveler speed U (*a* according to *Lüdicke*, *b* according to Stein, *c* according to *Meister*, *d* according to *Escher*, 1 traveler and ring dry, 2 oil lubricated)

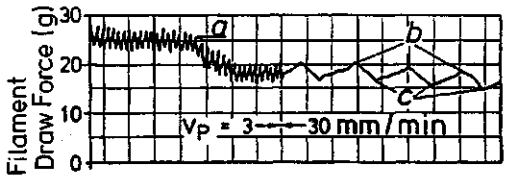

Figure 3.53 Time relation of the filament tension during ring twisting (v_P = chart speed, *a* = ring oil lubricated, *b* = pirn cone tip, *c* = pirn base)

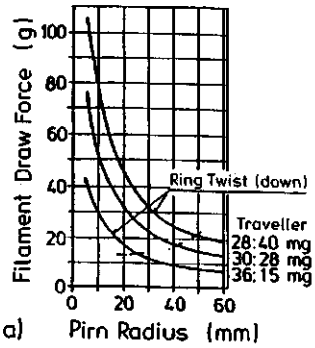

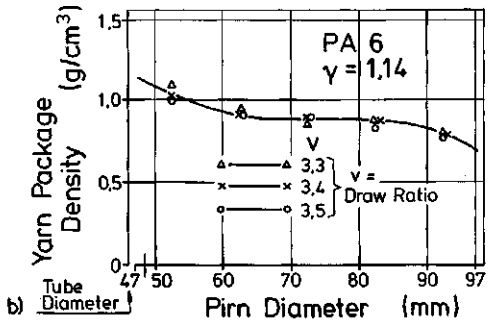

Figure 3.54 *a*) Thread tension during ring twisting between traveler and pirn for $n = 10{,}000$ rpm, balloon height $A = 400$ mm, ring diameter $D = 120$ mm, titer = 60 den, traveler friction coefficient $\mu = 0.7$
b) Yarn package density for PA 6 ($\gamma = 1.14$ g/cm^3) under the conditions of a)

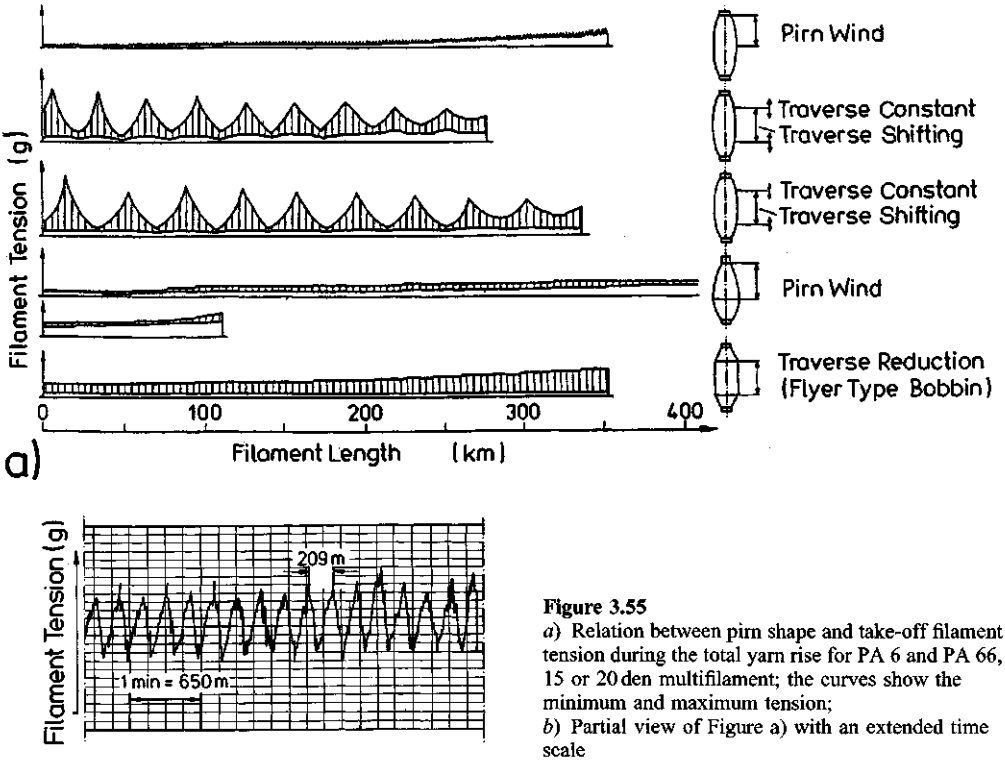

Figure 3.55
a) Relation between pirn shape and take-off filament tension during the total yarn rise for PA 6 and PA 66, 15 or 20 den multifilament; the curves show the minimum and maximum tension;
b) Partial view of Figure a) with an extended time scale

According to [82] the draw ratio and the cops diameter D have also some influence on the packing density of the yarn: A change in draw ratio from 3.3 to 3.5 results in a 3 . . . 5% higher packing density than in the cops inside layers (i.e., in its top) can also be 10 . . . 20% higher than in the outside layers.

The take-up tension and the packing density as well as the altered shrinkability (altered by the packing density) influence the take-off tension [83] that according to Fig. 3.55 is much more favorable for the lower two cops shapes than for the upper three cops shapes, i.e., with the upper layers the pirn wind has the lowest tension and tension variation.

3.9 Draw and Holding Forces for Filament and Tow

Filament and tow are delivered by rolls (drums, godets) into drawing or similar zones or drawn from these. The possibilities for this are shown in Fig. 3.56a–d. For the calculation of the forces the following is valid:

$$S_n = S_0 \cdot \sum_{1}^{n} e^{\mu_n \cdot \alpha_n} \tag{3.27}$$

S is the tension of the filament or the tow, index 0 for the input and n after the nth drum or at the take-off, μ is the coefficient of friction and α (in the arc) = the wrapping angle. The course of the yarn from a–c is only suitable for filaments up to several 10^3 tex, while d has also been used for up to 10^6 tex. The limitation is in the yarn running width plus some safety distance (for a–c); d is only limited by the

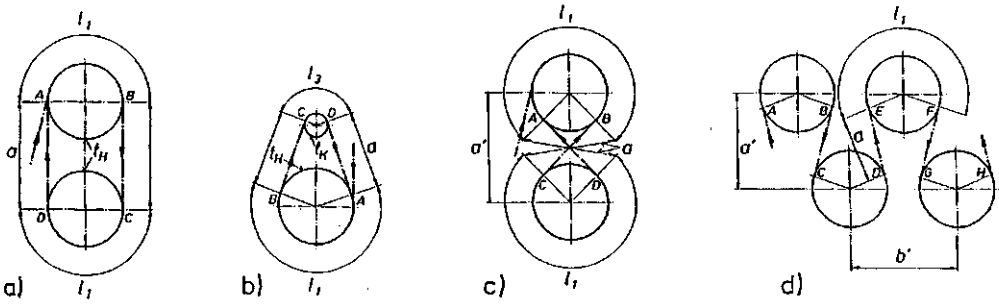

Figure 3.56 Yarn guidance for different godets or drum arrangements:
a) Godet duo with outside wraps
b) Godet with idler roll
c) Godet duo with crosswise wraps
d) Multi-drum parallel roll work

mechanical strength and the length of the drums. Figure 3.57 shows an example for the running width of a 10,000 dtex multifilament and Table 3.11 an overview over the useful tow running widths.

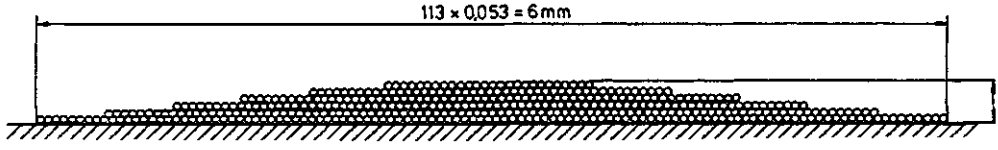

Figure 3.57 Multifilament width over the godet duo or over several parallel rolls (total 10,500 dtex, Rieter AG, see Figure 4.197 M2)

Table 3.11 Practical Tow Running Widths

Tow den	tex	Tow diameter compact mm	Tow diameter mm	Cable thickness × width mm^2
5000	556	0.78	1.32	0.1 × 14
10000	1110	1.1	1.85	0.1 × 27
40000	4440	2.2	2.7	0.15 × 39
100000	11110	3.5	6	0.4 × 70
150000	16670	4.7	7.2	0.5 × 82
200000	22220	4.9	8.3	0.6 × 92
300000	33330	6	10.2	0.75 × 110
500000	55550	7.8	13	1 × 134
10^6	111100	11	18.7	1.3 × 210
$n \times 10^6$	111100 n			$\approx n \times 1.3 \times 210$

The material dependent coefficient of friction (see Chapter 6.7 and 7.2) between relatively dry tow and a hard chromed or hardened drum surface without any movement relative to each other $\mu \approx 0.4$ and with movement relative to each other i.e., sliding, 0.1 ... 0.2 and can reach for wet tow up to 0.8.

For Fig. 3.56a the formula (3.27) is reduced to $S_n = S_0 \cdot e^{2n\pi\mu}$. The arrangement *c* does give a larger wrapping angle, but is rarely used due to the operating problems. If one wrap is added to the front by hand in *a* or *b*, the remaining wraps form automatically. The wrapping distance sets itself due to the angle of the roll axis (Chapter 7.6).

For d it is possible that $S_n > S_{n-1} e^{\mu n}$, and then the tow slides on the nth drum. This hot draw plate effect is used in praxis (see Fig. 2.63). If the tow is supposed to run smoothly it is useful to increase each drum diameter at constant rpm by 0.1 ... 0.2% unless the tow shrinks during the passage. Onto a low tension tow intake or output it is useful to add a free running rubber coated pressure roll. For a low tension tow running off the last drum this roll has a dulled surface ($R_t < \approx 2\,\mu m$), while other drawing rolls are better smooth ($R_t \approx 0.2 \ldots 0.4\,\mu m$).

Table 3.12 gives an overview over the tow tensions at the output roll according to Fig. 2.63 with low input tension from the left and an output tension of $S_7 = 1000$ kg for different coefficients of friction. It becomes obvious that the major tension jump is between the drums 4 and 6, i.e., in the humidifying trough.

Table 3.12 Tow Tension at the Output Roll according to Fig. 2.63

μ	S_n	S_{n-1}	S_{n-2}	S_{n-3}	S_{n-4}	S_{n-5}	
0.4	1000	480.4	110.9	25.6	5.9		kg
0.2		693.1	330.0	160.0	76.9		kg
0.4				→ 133.2	→ 92.3	23.1	kg
0.1		832.6	577.1	400.0			kg
			↑ Wet roll			$n=7$	

The necessary drive and holding powers in the individual drawing zones can be calculated from

$$N[\mathrm{kW}] = N_0 \cdot n[\mathrm{rpm}] + (S_n - S_0) \cdot v[\mathrm{m/min}]/60 \cdot 102 \cdot \eta \approx S[\mathrm{kg}] \cdot v[\mathrm{m/min}]/6120 \cdot \eta \qquad (3.28)$$

For the individual efficiencies see Chapter 4.13.6.

3.10 Contact Heating and Drying of Filaments

Here the same yarn and tow guidance forms as in Fig. 3.56a–d are valid. From the cross-sectional view through the running filament bundle it becomes clear that the outer layers stay cooler than the inner contact layers unless the filament or tow bundle is continuously turned as in Fig. 3.56c and/or the heated drum system is not encapsulated in an isolation chamber of the same air temperature.

A calculation of the yarn heating or cooling by heated or cooled godets is possible with the following equations [37]:

for hot godet duos	for hot godets with idler rolls
$T_1 = T_H - (T_H - T_\lambda) \cdot \exp\left(-\frac{K_w \cdot l_1 \cdot \alpha_1}{v \cdot \sqrt{Tt}}\right)$;	$T_1 = T_H - (T_H - T_\lambda) \cdot \exp\left(-\frac{K_w \cdot l_1 \cdot \alpha_1}{v \cdot \sqrt{Tt}}\right)$
$T_2 = T_K + (T_1 - T_K) \cdot \exp\left(-\frac{K_w \cdot l_2 \cdot \alpha_2}{v \cdot \sqrt{Tt}}\right)$;	$T_2 = T_K + (T_1 - T_K) \cdot \exp\left(-\frac{K_w \cdot l_2 \cdot \alpha_2}{v \cdot \sqrt{Tt}}\right)$
$T_3 = T_H - (T_H - T_2) \cdot \exp\left(-\frac{K_w \cdot l_1 \cdot \alpha_1}{v \cdot \sqrt{Tt}}\right)$;	$T_3 = T_K + (T_2 - T_K) \cdot \exp\left(-\frac{K_w \cdot l_3 \cdot \alpha_1}{v \cdot \sqrt{Tt}}\right)$
$T_4 = T_K + (T_3 - T_K) \cdot \exp\left(-\frac{K_w \cdot l_2 \cdot \alpha_2}{v \cdot \sqrt{Tt}}\right)$;	$T_4 = T_K + (T_3 - T_K) \cdot \exp\left(-\frac{K_w \cdot l_2 \cdot \alpha_2}{v \cdot \sqrt{Tt}}\right)$

(3.29)

with

$T_1, T_2 \ldots T_n$ = Yarn temperature T_F after passing through the individual heating or cooling zones

α_1 = Heat transfer coefficient of the metal surface–yarn system (assumed equal for heating and cooling)

α_2 = Heat transfer coefficient for the yarn–air system

l_1 = Contact zone of the yarn with the heated godet surface (for A I and A II different length due to the different yarn guidance geometry, see Fig. 4.73)
l_2 = Air zone of the yarn (for A I and A II different length due to the different yarn guidance geometry, see Fig. 4.249)
l_3 = Contact zone of the yarn with the surface of the spreader roll
Tt = Yarn titer
v = Yarn speed
Z = Number of wraps of the yarn around the geometrical arrangement (one wrap = length of the way ABCDA)
K_w = 0.056 for PA
= 0.076 for PET
= 0.047 for PP
= yarn material specific constant for the heat transfer.

According to this it is possible to calculate for the heat transfer in moved air to the yarn about 50 ... 200 W/m² K and on metal contact surfaces about 450 ... 600 W/m² K (higher values for finer yarns and higher speeds). Figure 3.58 shows a sample calculation for this (due to the large number of sequential equations best with a computer), A I for the duo *a*, A II for the godet with the idler roll *b*. In both cases the desired yarn temperature is achieved after two wraps. The decline in between is due to the air zone respectively the air zone and idler roll.

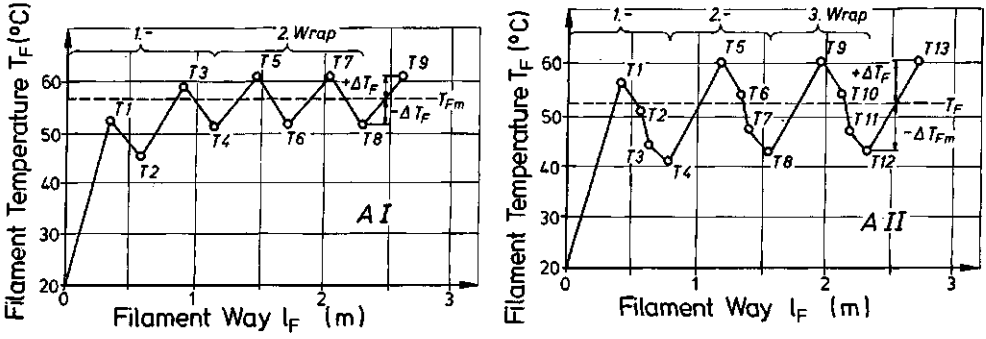

Figure 3.58 Principal heating and temperature development for a filament on hot godets with arrangement according to Fig. 3.56a (A I) respectively b (A II) (l_F = filament way) [84]

If this calculation seems too difficult, it is possible to use the following approximation that is equal for the duo and the godet with idler roll. The necessary yarn contact length becomes

$$L_{contact}[m] \approx k \cdot 10^{-8} \cdot v[m/min] \cdot Tt[dtex] \cdot \Delta T_{yarn}[°C] \tag{3.30}$$

with $k \approx 0.6$ for dry and $k \approx 1.0$ for lubricated multifilaments. After $L_{contact}$ the final temperature difference between drum surface and outgoing yarn becomes $< 2 \ldots 3$ °C (or K).

Drying measurements on viscose rayon with an initial humidity of about 400% to a residual humidity of $\approx 0.3\%$ for 60 ... 265 dtex multifilaments could be interpolated to $\partial f / \partial n = 24.4 \cdot p_D / v\tau \pm 8\%$, leading generally for contact drying to [85]:

$$L_{contact}[m] \approx k_W \cdot 10^{-4} \cdot f(100 = 1) \cdot v[m/min] \cdot Tt[dtex] / \Delta p_D \tag{3.31}$$

with Δp_D = partial water vapor pressure difference between the yarn surface and the dryer atmosphere and $k_W \approx 0.8$ for water. If the drums are not internally heated but only by the surrounding air, the formulas are only valid as long as the heat transfer from the air to the drums is sufficient to cover the drying heat requirement of the yarns, i.e., the free yarn spacing has to be at least about twenty times the yarn running width.

If the distance $a \gg D$ (according to Fig. 3.56a respectively d) one can assume mostly air heating or in the case of unheated drums exclusively air heating of the yarns, and the heat transfer to the yarns has to be calculated with $\alpha \approx 50 \ldots 200\,W/m^2\,K$.

When arranging several drums very closely to each other or to a wall it is necessary according to the German safety regulations to keep the minimum surface distance of 120 mm.

3.11 Stuffer Box Crimping

Here large and largest yarn bundles or tows are textured in a bent (in the individual filament in one plane) shape to achieve higher adhesion and volume during the later mechanical spinning process. According to Fig. 3.59 this effect is created because the filaments are pressed through the rolls for transport and tend to follow one roll surface and stick to the other as soon as the bending rigidity has been passed, etc. If L is the bending length and L_g is the periodicity (usually between 3 and 6 mm [86]), the crimp becomes $EK = (2L - L_g)/2L$. The counter force is created in the stuffer box by the friction of the filament bundle against the walls (Fig. 3.60) and continuously decreases towards the tow exit. It can be deduced from the second order bend differential equation with E = elastic modulus and J = inertia of the bending cross-section to $P_K = \pi \cdot E \cdot J/4 \cdot L^2$. For the inertia of a round PET filament cross-section as an individual filament $J = 0.0322 \cdot 10^{-12}$ [dtex]^2, resulting in $P_K = 0.08 \cdot 10^{-12}$ [dtex]$^2 \cdot E/L^2$. For a bending filament sliding in an also bending filament bundle $P_K \leq P_K^* \leq 2P_K$. The exact determination is difficult because it depends on the filament adhesion and friction to the neighboring filaments that in turn depends on the packing density of the yarn, their surface roughness, and the adhesion of the lubrication; thus it is not definable within these limits. The elastic modulus of standard PET fibers at 20 °C is about 35,700 kg/mm^2, at 98 °C about 12,000 kg/mm^2, and at 150 °C only 8000 kg/mm^2 ($\approx$82 dN/mm^2).

The counter pressure P_K is built up by the friction of the crimped filaments on the stuffer box walls and generally results in secondary crimping because of the box width, also shown in Fig. 3.60. The bending work in the area of the bend is transformed into heat that due to the low heat conductivity of the filament bundle stays in the close vicinity. Under these conditions one can calculate the highest box pressure; Fig. 3.61 shows some sample results. For $P_K^* = P_K$ it follows that standard PET tow with

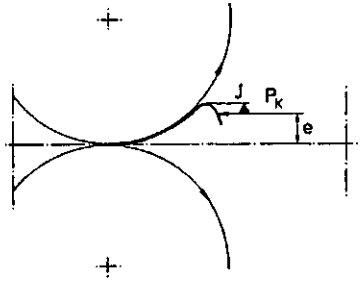

Figure 3.59
Explanation of filament bending for stuffer box crimping

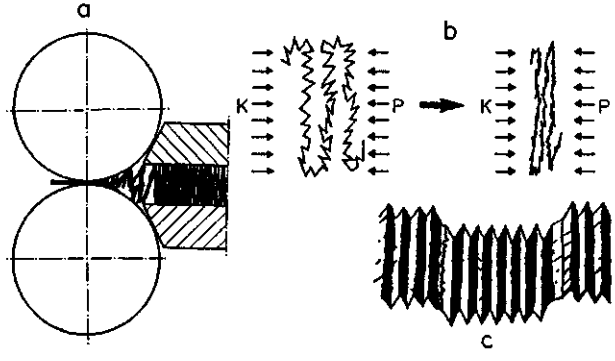

Figure 3.60
Formation of the primary and secondary crimping in a stuffer box process
a) Formation of the micro and macro crimp in the wedge between the two stuffer box rolls (macro crimp $\approx$ half the chamber height)
b) Direction change of the micro crimp to either side by high pressure from both sides (K = tow supply pressure, P = package counter pressure)
c) Typical crimp image with different side bows

1.25 ... 2 dtex and box temperatures of $< \approx 60\,^{\circ}C$ can be crimped well, while HM-HT-PET-tow needs $> 150 \ldots 200\,^{\circ}C$ for this; this means that for this heat the necessary heat setting effect on the previous calander rolls is practically removed, increasing the breaking elongation.

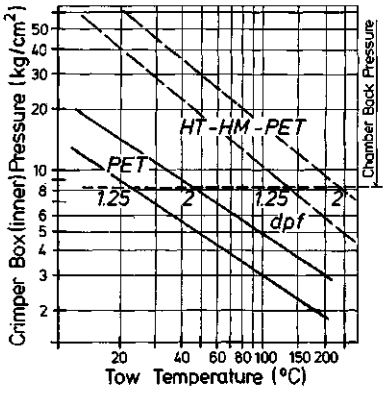

Figure 3.61
Results of 2 sample calculations for the relation between stuffer box counter pressure and the temperature in the chamber for PET tow

The elastic modulus of the fiber material can be reduced by injection of water vapor. If this vapor comes close enough to the bends of the tow, the fiber temperature needed for the crimping can be reduced. This is also true for tow steaming just in front of the stuffer crimp rolls; however for the usual technical tow at least 0.5 s steaming time with 100 °C saturated vapor are needed. Condensation drops on the tow have to be avoided because they would interfere with even dyeing.

3.12 Heat Setting

Just like steel can be geometrically deformed and then stabilized in this new shape by heating and cooling, synthetic fibers and fabrics can be heat-set at polymer specific temperatures. The need to create form stable and wrinkle resistant fabrics caused the development of heat setting between 1948 and 1950 at several places [87–92]. Figures 3.62 and 3.63 demonstrate the effect of boiling on not heat set (left) and on heat set (right) samples [89]. A simple model analysis of the inter-molecular processes is shown in Fig. 3.64 [93]: The hydrogen bonds always try to achieve an energy minimum; this is easy after an appropriate increase in temperature. This new state is then frozen by cooling.

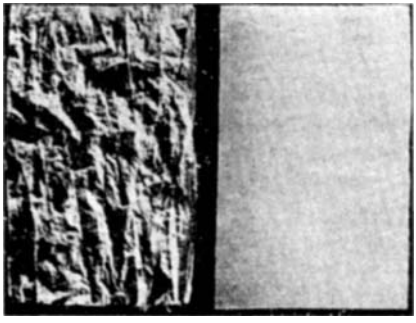

Figure 3.62 PA 6 fabric, right optimum heat-set, left non-heat-set, after three hours in boiling water and subsequent tension-free drying

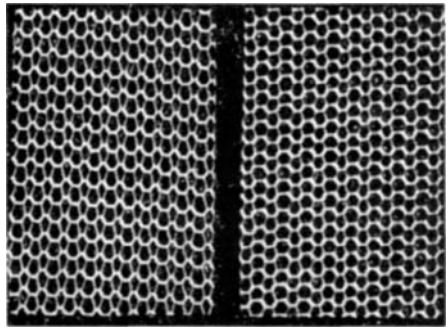

Figure 3.63 Photo of a PA 6 hosiery, right heat-set on a support, left not heat-set (the effect of the heat-setting process is a uniform and stabilized mesh system)

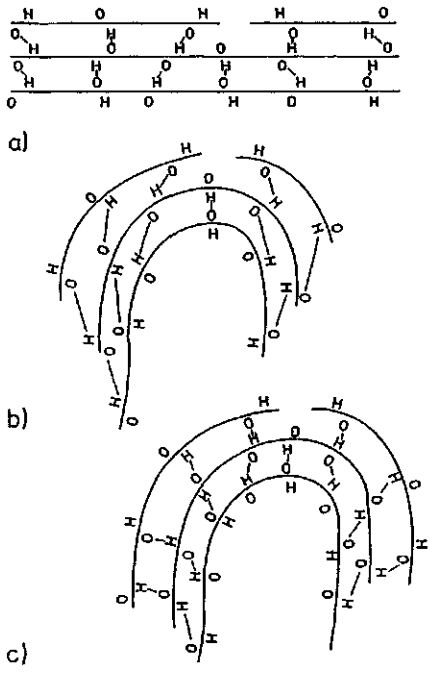

Figure 3.64
Schematic drawing of the intermolecular connections and their changes by heat-setting of PA 6 respectively PA 66:
a) Straight and not tensioned and not deformed PA 6 filament part (straight long lines = main chains, short lines (between O and H) = hydrogen bonds)
b) Filament partial view from a) mechanically deformed: the distances between O and H, i.e., the lengths of the hydrogen bonds became longer (e.g., like an expander: the inner tension increasing)
c) Filament partial as in b) after heat-setting: The hydrogen bonds did vibrate by heat back to the minimum distances at the energy minimum. This situation has to be frozen by cooling. When bending this filament in c) back to a straight filament as in a) the so reformed tension has to be heat-set again and cooled in the shape of a).

Swelling can create similar effects, because it increases the distance of neighboring O and H atoms by solvatation [92–94]. The removal of the swelling agent replaces the cooling.

3.12.1 Basics

Heat setting is more effective the more freely the hydrogen bonds can swing, i.e., the higher the temperature is. A certain tenacity—about 1 . . . 1.5 g/dtex—must however be maintained to avoid plastic deformation. Below the glass transition temperature there is no further effect. Figure 3.65 shows the most important temperatures for thermal treatment of some synthetic materials. The optimum heat setting temperature may not be significantly passed.

In the production process heat setting is practically necessary after each mechanical deformation to relax the respective deformation state. Thus the first heat setting, e.g. a twist relaxation, should be done at the lowest possible temperature: PA 66 twisted yarn can already be treated in 95 . . . 98 °C saturated steam, while PA 6 twisted yarn required 105 °C saturated steam, i.e. a vacuum/pressure vessel treatment. Preceding evacuation of the yarn packages is necessary to remove all air as it would prevent the even penetration of the water vapor.

From the energy spectra it can be concluded that dry heat setting at a certain temperature will be removed by a similar second treatment. Heat setting at 130 °C however is only covered 11.5% by a subsequent 100 °C treatment, all other conditions the same [91, 93]. The presence of swelling agents, e.g., saturated water vapor, changes these relations: Heat setting PA 6 twisted yarn or fabric in 130 °C saturated steam is equivalent to a 190 °C hot dry air treatment, however with different exposure times. The remaining differences have to be pointed out because they may be relevant for the choice of heat setting method:

- Yarn tension interferes with shrinking during heat setting: Higher yarn tension results in higher residual shrinkage as does a shorter heat setting time. During optimum saturated vapor heat setting the same product completely shrinks even at 0.5 g/den tension (Fig. 3.66).
- If the heat setting effect is measured by the achieved residual shrinkage, Fig. 3.67 shows with the example of a PA 66 woven fabric that certain exposure times are needed depending on the

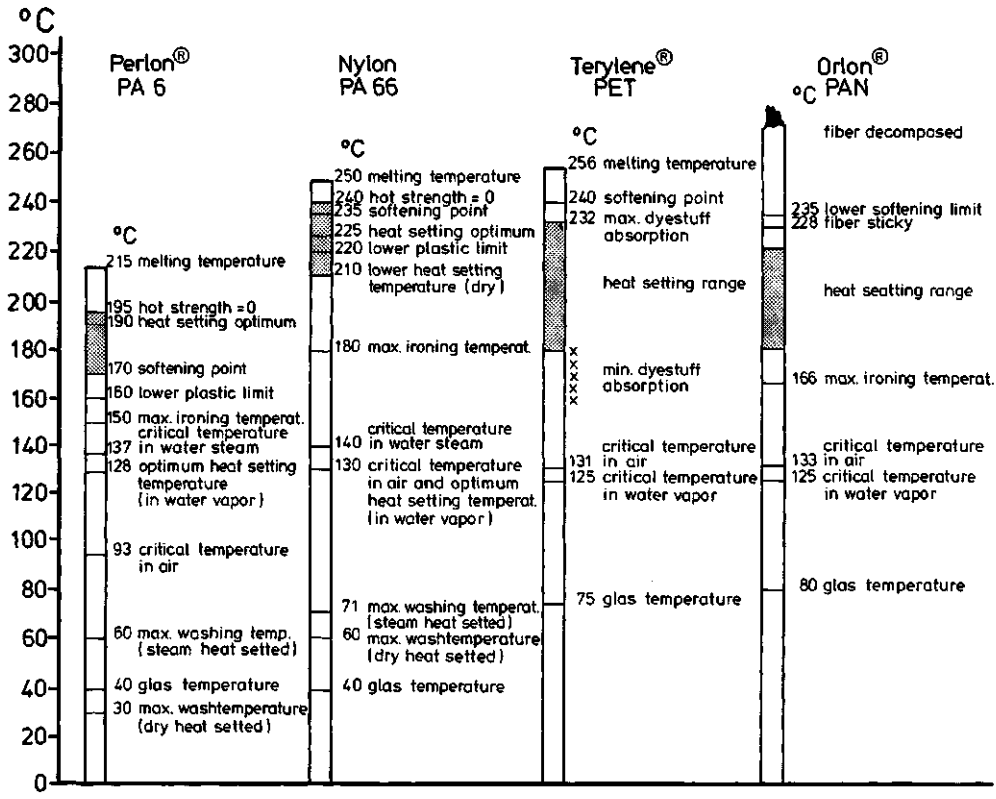

Figure 3.65 The most important temperatures for the thermal treatment of some synthetic filaments

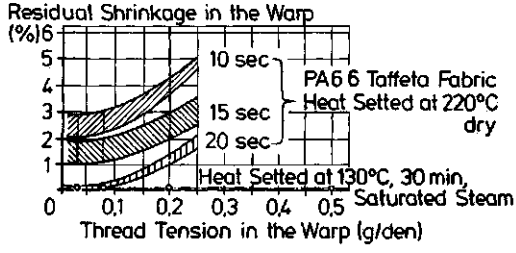

Figure 3.66 Influence of tension and time on the heat-setting result of a PA 66 taffeta fabric, dry heat-set at 220 °C: warp: PA 66—60 den, 300 S tpm, 42 filaments per cm; weft: PA 66—2 × 60 den—600 S tpm, 34 filaments per cm

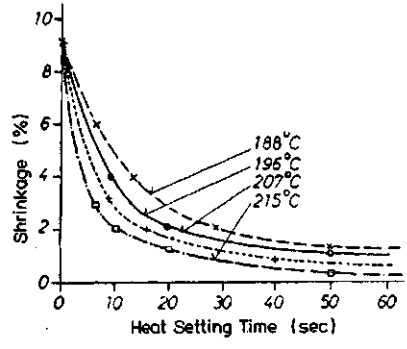

Figure 3.67 Time relation of shrinkage during heat-setting of PA 66 taffeta fabric in hot air

temperature, as is a minimum temperature. The required times are also depending on the thickness of the material: In draw texturing textile yarns of 40 ... 167 dtex only ms are available for the inside of the filaments to arrive at the heat setting temperature and to cool down again.

- The crimp (relaxation) angle α is also depending on the material, the process medium, and the temperature (Fig. 3.68). Only in the vicinity of the optimum heat setting temperature after the appropriate time a sufficient effect can be achieved, as is with the help of a swelling agent at the appropriate temperature for a specific material.

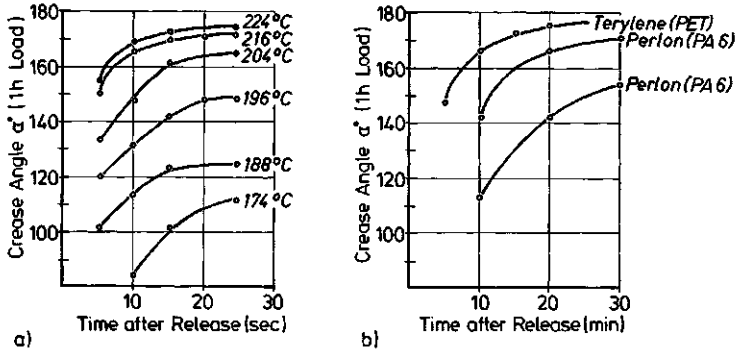

Figure 3.68
a) Crease angle of PA 66 taffeta fabric after air heat-setting
b) Crease angle of Terylene and Perlon taffeta fabric after chemical treatment with o-phenol sulfuric acid water solution of 80 °C

- The density and dyeability are also influenced greatly by heat setting. While for PA 6 and PA 66 the density increases with increasing heat setting temperature, it remains almost unchanged for PA 12. In all cases there is a difference between cold and hot drawn material.
- The dyestuff affinity increases strongly with growing steam afore heat setting temperature with free shrinkage in the case of the above mentioned polyamides. When heat setting under constant length this influence is very weak or disappears totally (Fig. 3.69). For PET the dyestuff absorption reaches a minimum after heat setting at 180 °C and increases at higher temperatures to about 2.3 times the original value.

The mentioned treatments as drawing, heat setting, and shrinking have great influence on the finished goods. So do even small variations in these parameters.

3.12.2 Heat Setting Processes for Synthetic Yarn and Fiber Production

For the practical application mostly three treatments are useful:

In dry hot air or superheated steam, or on hot rolls or plates or in saturated steam.

For heat setting in saturated steam [95] tow or staple fibers are evacuated several times in cans or yarn bobbins on a support car inside a jacket heated pressure and vacuum vessel to < 100 mm water column and saturated steam inflow (depending on the material and the heat setting method between 100 and 135 °C) and then steamed for about 15 ... 45 min and then evacuated again. To achieve even lots it is recommended to use process programming. Sediment traces of iron derivates on the outer layers of the yarn can be avoided by letting the steam flow in through a filter from the same fiber material and a vessel from material 1.4541 (≈AISI 304). Condensation drops can be avoided by steam jacket heating.

For hot air setting to stabilize crimp and to shrink to a residual shrinkage of < 0.5% the tow has to be without tension, e.g., by laying the cable in meander shape onto a belt or onto a perforated cylinder with air suction to the inside [99]. If the treatment times according to Fig. 3.70 are applied with subsequent cooling to below the glass transition temperature, the effect will be sufficient. However, breaking elongation will be at a maximum.

If the tow is only drawn under high tension, then possibly crimped and dried, there will be a residual shrinkage. For PAN it can be up to about 40%. If 40 ... 60% of such high shrinkage staple fibers are blended with 60 ... 40% completely shrunk fibers and spun mechanically, subsequent shrinking will cause the low residual fibers to crimp due to adhesion; the result is the high volume "high bulk staple yarn" [101].

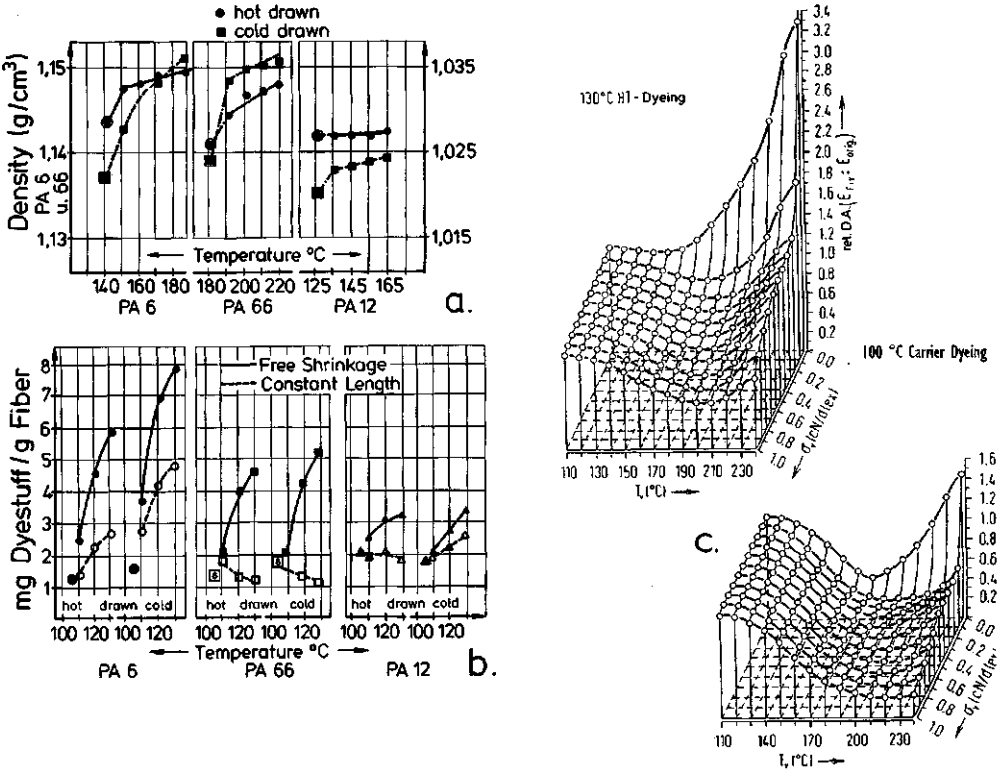

Figure 3.69 *a*) Influence of the heat-setting temperature on the density of PA 6, PA 66, and PA 12
b) Influence of the hot water vapor treatment during the drawing process on the dyeing process in comparison to cold drawn material for PA 6, PA 66, PA 12 (Dyestuff absorption in mg dyestuff/g fiber)
c) Influence of the heat-setting temperature on the dyestuff absorption of Terylene (dyeing bath with 2% "Dipersolecht scharlach" B 150, 90 min at 100 °C)

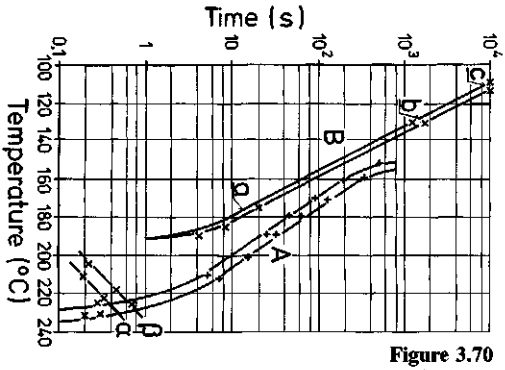

Figure 3.70
Optimum heat-setting time as a function of the heater temperature for (A) PET and for (B) PA 6

+ stuffer box crimped tow ($v = 200$ m/min)	*a* dry
x yarn for texturing	*b* in hot water steam
α *76 dtex*	*c* in water
β 167 dtex	

For the production of HM-HT-cotton-type polyester fibers the tow is set under high tension on large heated drums so that it cannot shrink and increases its breaking elongation. A PET-tow of about $2.1 \cdot 10^6$ dtex that is being set over 16 drums of 600 mm diameter with equal surface speed [99, 100] (with 200 m/min about 60 t/24 h) at 210 °C has an exposure time on these drums of about 6.3 s. The relatively even heat penetration of the about 1 mm thick tow is achieved automatically by turning the heated surface at the change to the next drum. The heat transport from the last heated drum to the first cooling drum is about 220 kW that have to be removed with this and the following cooling drums to lower the tow temperature at constant length below the glass transition temperature. After cooling it is led through a saturated vapor chamber of 100 °C to be prepared for stuffer box crimping. The higher the tow temperature on the heating rolls, the lower the residual shrinkage. The heat setting temperature may not exceed 230 °C, because this would lead to 3% residual shrinkage.

A stepwise small reduction in the drum circumference speed results in a lower residual shrinkage with an increase in breaking elongation.

In many cases a small residual shrinkage is advantageous for further processing.

In (draw) false twist texturing the filaments (usually between 40 and 167 dtex) are set with about 0.4 s contact time on the heating plates and then cooled on the cooling plates in a little shorter contact time. The twist effect remains in the yarn and turns into bulk during retwisting at the false twist element. In a second stage with higher temperature and defined draw this bulk can partially be removed and the yarn can be set in the new state; this creates set-yarn.

In the BCF yarn production the crimp is created by hot compressed air when impinging on a yarn plug, held in this shape at constant temperature and frozen when passed onto the vacuum cooling drum.

Tire cord that later undergoes another temperature treatment during vulcanizing is heat set directly after hot drawing on the third godet duo (see Fig. 4.63 and 4.197 *M*) at about 230 °C for PET and cooled on the fourth godet duo to under 60 °C.

3.13 Crystallinity

At least for PET chips intake of single screw extruders the crystallinity becomes clearly visible: Not crystallized PET adheres in the entry zone as soon as it reaches a temperature between 120 and 150 °C, forms an adhesive ring and blocks further chip intake. Also inside the yarns the amorphous and crystalline areas determine the fiber properties. Figure 1.1 shows that in the fiber structure amorphous and crystalline regions follow each other and are sometimes mixed. When heating, e.g., during heat setting, the adjacent chains sort by their orientation without changing it; this can be shown by X-ray analysis. The density increases as shown in Fig. 3.71 for differently drawn PET filaments. Curve (1) was measured on an undrawn material respectively granulate. The degree of crystallization can be calculated as

$$\alpha = (\gamma - \gamma_a)/(\gamma_k - \gamma_a) \tag{3.32}$$

(γ = density and index a for completely amorphous and k for completely crystalline).

The following densities follow from:

	PET	PP	PA 66	PA 6
γ_k	1.455	0.913	1.160	1.145 [g/cm^3]
γ_a	1.331	0.880	1.122	1.128 [g/cm^3]

Figure 3.72 shows the corresponding crystallinity of PP as a function of the draw ratio and Fig. 3.73 of different polyamides in dependence of the treatment temperature.

It also needs to be pointed out that the different methods of determining the crystallinity

- X-ray deviation
- Ultra red spectroscopy
- Caliometric
- Suspension method

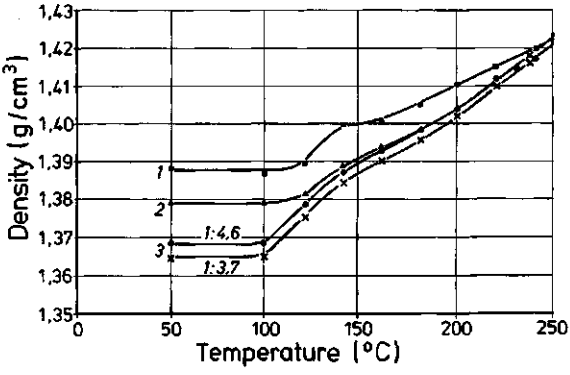

Figure 3.71
Density of differently drawn PET multifilaments as a function of the filament temperature after heat-setting for 30 min

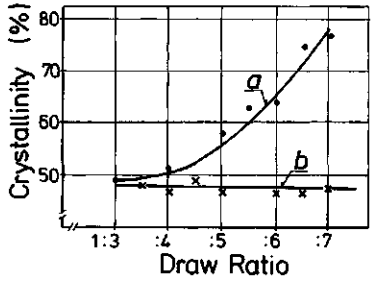

Figure 3.72 Relation between crystallinity α of polypropylene and the draw ratio when drawn over a hot pin or a hot plate
a) Measured by a pycnometer
b) Measured by x-ray deviation

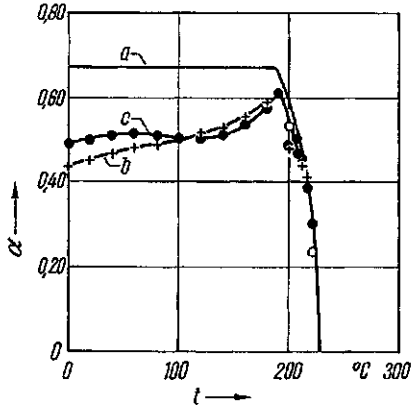

Figure 3.73 Estimated crystallinity of PA 6 as a function of the temperature [105];
a) Hot tempered
b) Filament, drawn
c) Filament, undrawn

result in different values, as shown in Fig. 3.72 for PP; therefore they cannot be compared to each other.

UV illumination lets crystallized PET chips luminesce white-blue, while non-crystallized PET remains dark gray.

References

1. *Gerres, H.:* Chem.-Ing.-Technik **52** (1980), p. 477
2. *Thiele, H.; Zettler, H.D.:* Auswahlkriterien für Reaktoren zum Herstellen von Polymeren, Kunststoffe **79** (1989) 8, p. 687
3. *Thiele, H.; Zettler, H.D.:* Bauformen von Reaktoren zum Herstellen von Polymeren, Kunststoffe **79** (1989) 9, p. 791
4. *Ludewig, H.:* VK-Verfahren, kontinuierliche Herstellung and Verarbeitung von Polyamiden, Berlin-Lichtenberg, 1 July 1942
5. Buss-Luwa AG, Pratteln/Switzerland

6. List AG, Pratteln/Switzerland
7. Werner & Pfleiderer, Stuttgart, Germany
8. *Ziabicki, A.:* Fundamentals of Fiber Formation, Wiley Interscience, New York, 1976
9. *Falkai, B. von:* Synthesefasern, Verlag Chemie, Weinheim, 1981
10. *Lückert, H.:* In Ullmann's Encyclopedia of Industrial Chemistry: Fibers, 3rd General Production Technology, VCH-Verlagsges., Weinheim, 1987
11. *Oshima, Y.* et al.: J. Chem. Soc. Kogyo Kagaku Zarshi **60** (1957) p. 311
12. *Ziabicki, A.*; et al.: Kolloid-Z. **198** (1964) p. 60
13. *Schurz, J.:* Lenzinger Berichte **10** (1961) p. 5
14. *Klare, H.; Fritsche, E.; Gröbe, V:* Svnthetische Fasern aus Polyamiden. Akademie-Verlag, Berlin, 1963
15. *Winnacker-Küchler:* Chemische Technologie, 3rd edition, 6, p. 626. Carl Hanser Verlag; Munich, 1973
16. *Fourné, F.:* Fadenkühlung beim Schmelzspinnen. CTI April 1978, p. 315
17. *Wagner, R. H. L.:* Hochgeschwindigkeitstexturierung von Garnen mit großem Titer, CTI, June 1974, p.475
18. *Brody, H.:* Hot Tube Spinning of Polyester Fibers, Paper 2nd International Conference on Man-Made Fibers, Beijing, China, Nov. 1987
19. *Langley, L. L.:* Concepts of spinneret design; Fiber Producer, April 1978, p. 14
20. *Shanholter, E.:* Spinneret Technology, Fiber Producer, April 1978, p. 52
21. *Eadie, D. D.:* Spinneret Design Calculations for Melt Spinning, Fiber Producer, April 1979, p. 40
22. *Haegler, G. E.:* Entry - Exit Effects in Capillary Flows of Polymer Melts and Solutions, Fiber Producer, April 1980, p. 8
23. Karl Fischer Industrieanlagen GmbH. Berlin, Taschenkalender 1990
24. *Dietrich,W.; Reichelt, G.; Renkert, H.:* Untersuchungen zum PES-Schmelzspinnprozeß bei Abzugsgeschwindigkeiten von 5000 ...10000 m/min., CTI, September 1982, p. 612
25. Hütte: Des Ingenieurs Taschenbuch: Ernst & Sohn: Berlin, 1955. 28th edition, p. 663
26. *Fourné, F.:* Blasschächte für die Faserherstellung, CTI September 1982, p. 604
27. *Köhler, P:* Berührungslose Bestimmung von Temperaturen und Durchmessern an einem aus Schmelze gesponnenen Faden, Chem.-Ing.-Technik **43** (1971) 5, p. 274
28. *Fourné, F.:* Unpublished research with 100 . . . 2000 single filaments and 500 ... approximately 4500 m/min take-up
29. *Lückert, H.; Stibal, W.:* Neuartige wirtschaftliche Technologien zur Produktion von PES-Fasern, CTI, January 1986
30. *Fourné, F.:* Fadenkühlung beim Schmelzspinnen (II), CTI April 1978, p. 320, Figure 10
31. DBP 3 414 602 (AD: 18. April 1984; *Fourné, F.*)
32. *Fourné, F.:* Einige Ursachen von Titer-, Dehnungs- and Färbeschwankungen, CTI 1984. p. 419
33. *Hilpert, R..:* Forschung **4** (1933) p. 215: An increase of turbulence from 0 to 2.5% increases the heat transfer coeficient by 80%; also see:*Reiber, H.:* VDI-Forschungsheft **269** (1925); Kestin, J.; et al.: ZAMP, **XII** (1961) p. 115; *McAdams, W. H.*: Heat Transmission, 3rd edition, New York, 1954
34. *Fourné, F.:* Blasschächte - Stand der Technik, CTI, 1987, p. 542
35. *Zachara, A.:* How to estimate the flow characteristics in multifilament spinning, Fiber World, May 1987, p. 13, and July 1987, p. 52
36. *Dutta, A.:* Role of quench air profiles in multifilament melt spinning of PET-fibers, Textile Research (Institute) J., January 1987, p. 13
37. *Bevreuther, R.:* Dynamik von Fadenbildungs- and Fadenverarbeitungsprozessen, Fachbuchverlag, Leipzig, 1986
38. Brit. Pat. 900 009 (AD: 19 April 1961 with US-Priority, 29 April 1960, DuPont)
39. *Prandtl, L.:* Strömungslehre, Vieweg & Sohn, Braunschweig, 4th edition, 1944
40. *Prandtl, L.; Oswatitsch, K.; Vieghargt, K.:* Führer durch die Strömungslehre, Vieweg & Sohn, Braunschweig, 8th edition, 1984
41. *Fourné, F.:* Synthetische Fasern, Wissenschaftliche Verlagsges. mbH, Stuttgart, 1964
42. *Böhringer, H.:* Gebrauchsoptimale Erspinnung von Chemiefasern; Veröffentlich. auf dem Gebiet der Faserstoff-Forschung and Textiltechnik, No. 8, Akademie-Verlag, Berlin 1957
43. *Tippetts, E. A.; Zimmermann, J.:* J. Appl. Polymer Sci. **8** (1964) p. 2465
44. *Schultze-Gebhardt, F.:* Colloid-Z. & Z. Polymere **236** (1970) p. 19
45. *Narisawa, I.;*et al.: J. Polymer Sci., Polymer Phys. Ed. **15** (1977) p. 1055
46. *Schultze-Gebhardt, F.:* Faserforsch. u. Textiltechnik-/Z. Polymerforsch. **28** (1977) p. 467
47. *Bonart, R.; Schultze-Gebhardt, F.:* Angew. Makromol. Chemie **22** (1972) p. 41
48. *Bobeth, W.; Reumann, R.-D.:* Wiss. Z. TU Dresden **24** (1975) p. 1091, Faserforsch. u. Textiltechnik **25** (1975) p. 233
49. *Winnacker-Küchler:* Chem. Technologie, 3rd edition, 6, p. 626. Carl Hanser Verlag, Munich, 1973
50. *Schultze-Gebhardt,F.:* in [4]

51. Swiss Pat. 631 311 and DBP 2 824 500 AD: 1978, *Stapp, H.*, in AKZO
52. *Fourné, F.:* Synthetische Fasern, Wissenschaftliche *Verlagsges.* mbH. Stuttgart. 1964, especially p. 482, 878
53. *Fourné, F.:* Fadenspannungen beim Zwirnen, Melliand-Textilber. **38** (1957) 5, 6, p. 488 and 602
54. *Georgi, G.:* Zwirne and Zwirnmaschinen; Konradin-Verlag Robert Kohlhammer, Stuttgart, 1957
55. *Fourné, F.:* Etagenzwirnmaschinen, Reyon (1958) p. 288
56. Barmag AG. Remscheid-Lennep, Germany
57. *Fourné, F.:* Stretch Yarn (Kräuselmaterial), Melliand-Textilber. **37** (1956) p. 661; **39** (1958) p. 247 and 361
58. DRP 618 050 (AD: 11. March 1932-: Heberlein & Co. Wattwil, Switzerland), additional patents see [1]
59. *Fourné, F.:* Stretch Yarn - die optimale Drehungszahl. Melliand-Textilber. **39** (1958.) p.135
60. *Lünenschloß, J.* et al.: Auswirkung der Spinngeschwindigkeit auf Simultanstrecktexturieung sowie Eigenschaften von FD-PES-Filamentgarnen und Rundstrickware; Forschungsvorhaben AIF No. 3788 at the Institut für Textiltechnik der RWTH Aachen; comprised report: Chemiefasern/Textilindustrie, February 1981, p. 135
61. *Artunc, H.; Weidörfer, H.:* Einfluß der Geschwindigkeit beim PES-Spinnen und des Fadenlaufprofils der Texturiermaschine auf das Verarbeitungsverhalten beim Texturieren. CTI, October 1988, p. 897, and Nov. 1988, p. 965
62. Barmag. Remscheid-Lennep, Germany
63. Giudici Davide + *Figli*, Sala Al Barro (CO)/Italy
64. ICB
65. Murata Machinery, Ltd., Kyoto/Japan
66. Rieter-Scragg Ltd., Macclesfield/UK
67. R.P.R., Oggiono (CO)/Italy
68. *Fourné, F.:* in Fourné Maschinenbau GmbH + Co. KG, 1978. Alfter-Impekoven
69. *Lünenschloß, J.; Fischer, K.; Bock, G.:* Theoretische Berechnung der Fadenoberflächentemperatur and des Temperaturgefälles im Fadenquerschnitt, CTI, June 1979, p. 463
70. *Wulfhorst, B.: Brunske, J.:* Stand and Entwicklung von Zwirn- and Texturiermaschinen, CTI, Januar 1988, p. 29
71. *Lünenschloß, J.; Fischer, K.:* Einfluß der Produktionsgeschwindigkeit auf Herstellung and Eigenschaften von technischen Polyestergarnen (II), CTI. Nov. 1978, p. 981
72. Barmag [6]: Brochure data
73. *Fischer, K. E.:* Ein Beitrag zur Torsions- and Strecktexturierung; Thesis at the Textile Institute at RWTH Aachen, November 1978
74. *Farber, K.:* Ein Beitrag zum Falschdrahttexturieren: Thesis at the Textile Institute at RWTH Aachen, 1986
75. *Rebsamen, A.:* Neuartige Möglichkeit des Spulenaufbaues dank Microprocessor, ITB, Garnherstellung. **3** (1988) p. 16
76. *Meyer, W.:* Die Präzisionskreuzspulmaschine, Sahm anniversary publication, Eschwege
77. Automatik-Wicklerbau, Hürth-Effern, Germany
78. *Lünenschloß, J.; Wiesel, W:* Das Spulenablaufverhalten in Abhängigkeit modifizierter Spulbedingungen, CTI, October 1988, p. 904
79. DPO 3 819 913 (AD 11 June 1988; Davy McKee AG, Frankfurt/Main)
80. *Fourné, F.:* Fadenspannungen beim Zwirnen, Melliand-Textilber. **38** (1957) p. 488 and 602
81. *Fourné, F.:* Determine Yarn Tensions with these Nomograms, Textile World, December 1957, p. 104 and 202
82. *Wegener, W.:* Der Einfluß des Verstreckungsverhältnisses auf die Schwankung der Fadeneigenschaften und der Ablauffadenzugkraft, Melliand-Textilber. **40** (1969) p. 261
83. *Lünenschloß, J.; Péterfi, M.:* Die Untersuchung des Aufbaues von Streckzwirncopsen, Textil-Praxis, December 1964, p. 1179
84. *Erdmann, W.:* Unpublished report; valid for drums in heat insulated housings with $T_{air} \approx T_{drum}$
85. $\Delta p_D = p_W$ (vapor pressure at drum temperature) $-p_R$ (partial vapor pressure in the surrounding room)
86. *Ehrler, P; Mavely, J.: Kräuselung* von Polyester-Spinnfasern, Melliand-Textilber. **53** (1983) p. 99
87. *Mecklenburgh, G. K.; Shaw, S.; Peters, H.W.:* Die Entwicklung der Fixierung aus Ausrüstung von Nylon-Geweben, Reyon u. Zellwolle (1954) p. 413 and 473
88. *Hees, W.:* Ausrüsten and Färben von Polyamid-Seidengeweben, Melliand-Textilber. **32** (1951) p. 542
89. *Fourné, F.:* Heißfixieren von vollsynthetischen Fasern, Melliand-Textilber. **33** (1952) p. 643 and 753
90. *Fourné, F.:* Die Fixierung vollsynthetischer Fasern durch Wärme: De Tex **11** (1952) p. 466 and 473
91. *Fourné, F.:* Synthetische Fasern. Konradin-Verlag. Stuttgart. 1953
92. *Fourné, F.:* Erfahrungen beim Heißfixieren vollsynthetischer Fasern, Textil-Praxis (1952) p. 644; (1953) p. 795; (1955) p. 217; (1957) p. 797, 898 and 1014
93. *Fourné, F.:* Synthetische Fasern, Wissenschaftl. Verlagsges. mbH, Stuttgart, 1964, p. 639
94. *Rath, H., Groschopp, H.:* Über die Einwirkung von Quellmitteln, insbesondere Phenol auf Polyamidfasern,

Textil-Praxis, Sept. 1957. p. 904
95. Ph. Welker GmbH + Co. KG. Lambrecht/Pfalz, Germany
96. Ed. Erdmann-Elektrotechnik. Mülheim-Ruhr, Germany
97. Rieter AG. Winterthur/Switzerland
97a. Barmag AG, Remscheid, Germany
98. Dienes Apparatebau GmbH, Mühlheim/Main, Germany
99. Fleissner GmbH + Co., Egelsbach, Germany
100. Neumag GmbH, Neumünster, Germany
101. Superba SA, Mulhouse/France
102. *Köhler, W. D.:* Thermisches and hydrothermisches Verhalten von Polyesterstoffen und deren Nutzanwendung für die Veredlung, Deutsche Textiltechnik **11** (1961) p. 653
103. *Ludewig, H.:* Polyesterfasern. Akademie-Verlag, Berlin, 1975, p. 383
104. *Ahmed, M.:* Polypropylene Fibers - Science and Technology, Elsevier Scientific Publishing Company, Amsterdam, 1982
105. *Schwartz, E.:* in *Viehweg, R.*, and *Müller, A.:* Polyamide, Kunststoffhandbuch VI. Carl Hanser Verlag, Munich, 1966
106. *Fourné, R., Czase. E., Mears, R.:* Ein anderes Schnellspulkopf-Konzept, CTI 41/93, September 1991, p. 1002
107. *Berndt, H.-J.:* Dissertational thesis at the RWTH Aachen 1971, Textil-Industrie **73** (1971) p. 879
108. Div.: CTI 1992/93